# GENETIC DISSECTION OF *lin-11* REGULATION IN DIFFERENTIATION OF *C. elegans* AMPHID SENSORY NEURONS

By

Siavash Amon, B.Sc

A Thesis

Submitted to School of Graduate Studies

in Partial Fulfillment of the Requirements

for the Degree

Master of Science

McMaster University

MASTER OF SCIENCE (2012) McMaster University

(Biology) Hamilton, Ontario

TITLE: Genetic dissection of *lin-11* regulation in differentiation of *C. elegans* amphid sensory neurons

AUTHOR: Siavash Amon, B.Sc (University of Waterloo)

SUPERVISOR: Professor Bhagwati P. Gupta

NUMBER OF PAGES: 83 pages

This thesis is dedicated to my family.

**Abstract**

The expression of *lin-11* is regulated by enhancers located upstream from, as well as within, *lin-11* intronic sequences. Multiple regulatory inputs control the spatiotemporal expression pattern of *lin-11*. To better understand that process, we have investigated these regulatory enhancers by dissecting two of the biggest intronic sequences of *lin-11*: intron 3 and intron 7. Using microscopy, we show that the expression of intron 3 is required in ten head sensory neurons and that the expression of intron 7 is required in two head neurons. The truncation of intron 7 revealed that its regulatory sequence may be located within its narrow 98 base pairs (bp) region. We used bioinformatics to predict which putative transcription factor(s) may regulate AVG expression. Using a hypersensitive RNAi mutant strain, *eri-1; lin-15b*, we tested forty putative transcription factors and quantitated the number of animals in which the molecular marker *lin-11*::GFP expression is knockdown in AVG interneurons.

Using electrotactic behavioral analysis we show that the speed of *lin-11* null allele, n389, is reduced by almost 50%, when compared to that of the wildtype animals, due to amphid sensory neuronal deformities. We determine which conserved domains of *lin-11* are required for the proper development of the neuronal and vulval cells via microinjection rescue experiments.

We sequenced eleven *lin-11* alleles to determine which conserved domains are affected and the role of each of these domains in the development of vulval and neuronal cells. Our findings suggest that all *lin-11* conserved domains are required for proper vulval cell differentiation as well as for proper development of the amphid sensory

neurons. Finally, using tissue specific markers we label vulval cells in *lin-11* mutants to show that those cells are defective, as judged by the lack of fate-specific markers in the vulval cells.

**Acknowledgments**

First I would like to thank my supervisor, Dr. Bhagwati Gupta, for his guidance and patience during this past two years. I could not have finished this thesis without your help and support. You have always challenged me and pushed me to become a better researcher, and more importantly to become a better person. Furthermore, I am very grateful to my committee member Dr. Roger Jacobs for his advice and guidance.

Next, I would like to thank and dedicate this thesis to my family for sacrificing everything to send me to school to become a better person. Thank you my lovely mother, Homaira Amon, for listening to me when things were not working out for me, and you always told me to be patient during the difficult times, because there would be a light at the end of the dark tunnel. Thank you my dearest father, Keram Amon, for believing in me and for working so hard every day to send me to school; you have sacrificed your whole life for me and your family, and for that, I cannot thank you enough. And finally, I would like to thank my two supportive younger brothers, Mansoor and Jaihoon for being great friends, and more importantly for encouraging and believing in me every day. I cannot express in words how much I love you all.

Also, I would like to thank all past and present colleagues in Gupta's lab for your help, encouragement, and patience in the past two years. I could not have finished this thesis without your support. There were times when things in the lab did not work out for me, and you guys were always there for me to support me and encourage me to be patient and to believe things would work out, and for that I am very grateful. Unfortunately, there are far too many people to name here due to space constraints. So once again thank you everyone in Gupta's Lab.

Finally, I am also very grateful to Dr. Joanna Wilson and everyone else who helped me to edit my thesis. THANK YOU!!!

# Table of Contents

## Figure Legend

## Table Legends

## List of Abbreviations

*Cel- Caenorhabditis elegans*
*Cbr- Caenorhabditis briggsae*
*C.re- Caenorhabditis remanei*
*C.bre- Caenorhabditis brenneri*
AC- Anchor cell
AVG- Anterior ventral neuron G
VPC- Vulval precursor cell
Pn.P – Ventrolateral P cell epidermal progeny
L1 to L4 – Larval Stages
Hyp7- Hypodermal syncitium
Utse- Uterine-seam cell connection
Egl- Egg laying defect
Vul- Vulvaless
Muv- Multivulva
Dpy- Dumpy
GFP- Green Fluorescent Protein
Pvl- Protruding vulva
Unc- uncoordinated
PCR- Polymerase Chain Reaction
RNAi- RNA interference
TF-Transcription Factor
Pro- Proline rich domain
LIM- Domain (*lin-11, isl-2, mec-3*)
HD- Homeo Domain

# Chapter 1- Introduction

## 1.1 *C. elegans* as a model organism to study the genetic bases of development and gene function

In 1974, Sydney Brenner established *C. elegans* as a model system for the study and development of neurobiology; subsequent development has led to many important discoveries and advances in the field of genetics. *C. elegans* has a simple anatomy: it has a tubular body and a hyperdermal wall enclosing the nerve, muscle, hypodermis, intestine, and gonads (Sulston and Horvitz, 1977). These animals have transparent cells that can be visualized using a simple differential interference contrast (DIC) microscope. This attribute is beneficial because it allows for the study of cell specific markers as well cell migration, which occurs during this animal's different developmental stages (Sulston and White 1980). Moreover, *C. elegans'* compact genome, consisting of more than 20,000 coding genes, has been sequenced and its complete cell lineage has been mapped (Kimble and Hirsh, 1979; Sulston et al., 1983).

Developmental events occur due to the spatial and temporal regulation and expression of specific genes, both of which result in complex cell signaling that allows for the differentiation of cells into specific tissues (Inoue et al., 2005). This communication is made possible by transcription factors that target specific cells that contain the receptors for a specific protein. Some transcription factors are regulated by many genes – this is also known as global level transcription regulation, as in the Hox gene *lin-39,* which is regulated by the *Wnt* and *RTK/Ras* signaling pathways – while

others are regulated at the tissue-specific level; the latter is the case for *lin-11* (abnormal cell LINeage-11), which is required for the proper function of vulva precursor cells (Eisenmann et al., 1998; Freyd et al., 1990; Gupta et al., 2002 Inoue et al., 2005; Wagmaister et al., 2006).

The expression of LIM-homeodomains (LIM-HD) proteins are important in tissue patterning and differentiation, as well as in neuronal patterning (Hobert & Westphal, 2000) and, specifically, in thermosensation. There are seven *C. elegans* LIM-HD proteins; based on conserved features within the homeodomain, and as shown in Figure 1, at least one of these falls into each of the six subclasses of the LIM-HD family (Hobert & Westphal, 2000). As illustrated in Figure 1, these homeobox genes include: the thermotaxis gene (*ttx-3*), LIM domain family genes (*lim-4, lim-7, lim-6*), a *C. elegan* homeobox gene (*ceh-14*), a lineage defect gene (*lin-11*) and a mechanosensory abnormal gene (*mec-3*) (Hobert & Westphal, 2000). The role of each LIM-HD has been studied in detail and their phenotypes have been observed and reported.

The structure of the LIN-11 protein includes a novel cysteine-rich motif: C-$x_2$-C-$x_{17\text{-}19}$-H-$x_2$-C-$x_2$-C-$x_2$-C-$x_{7\text{-}11}$-(C)-$x_8$-C (Figure 2). This arrangement of cysteine residues, referred to as the LIM domain, is located in the *N*-terminal region of the protein and functions in metal binding and protein stabilization (Freyd et al., 1990; Hobert et al., 2000). The LIN-11 protein contains two conserved domains: LIM and HOX. More specifically, there are two LIM domains, LIM1 and LIM2, a Homeodomain (HD) and a Proline rich region (Pro), all of which are located at the C-terminal end. It has been

predicted that the spacing of paired cysteine and histidine residues, both of which are separated by two amino acids in LIM domains, suggests a function in DNA binding (Valle et al., 1991). It has been shown that LIM domains play a role in protein-protein interaction, and that that role may be responsible for the regulation of transcriptional events, which occur due to an increase in DNA specificity and affinity (Velyvis A & Qin J, 2000). The arrangement of cysteine residues in this motif, referred to as LIM, as well as similarly conserved structures, is seen in *mec-3* (touch neuron differentiation in C. elegan) and *isl-1* (rat insulin I gene enhancer-binding protein) (Freyd et al., 1990). DNA binding studies show that the conserved homeodomains are important for DNA binding and for proteins that regulate gene expression (Scott et al., 1989). Lastly, the function(s) of the proline rich domain are still unknown.

Three pairs of neurons, AFD, AIY and AIZ, play a key role in thermosensation, however, *ceh-14* is expressed in the AFD neuron, and a *ceh-14* mutant displays thermotactic deformities. The *ceh-14* is not required for the cell linage differentiation of AFD, AIY and AIZ neurons, but it is required in later developmental stages of those same neurons; in those later stages, *ceh-14* allows those neurons to function properly (Cassata et al., 2000). Similarly, two other LIM homeobox genes, *ttx-3* and *lin-11*, are required by the interneurons AIY and AIZ, respectively (Cassata et al., 2000). Thus, the three different LIM homeobox genes specify thermosensory neurons in *C. elegans* (Hobert et al., 1998; Mori, I. I., & Ohshima, 1995; Sarafi-Reinach et al., 2001). *mec-3* mutants are touch insensitive and *mec-3* is required for the proper differentiation of the six touch

receptor neurons, which include FLP, AVM, ALM, PVD, PVM, and PLM (Way et al., 1988; Xue, et al., 1992). *lim-7* null animals have very severe phenotypes including being uncoordinated, detached pharynx, and morphological defects (Voutev et al., 2009). It has been shown that the loss of *lim-6* function affects the two classes of GABAergic motor neurons that control rhythmic enteric muscle contraction (Oliver et al., 1999). The AWA, AWB, and AWC olfactory neurons are each required for the recognition of a specific subset of volatile odorants (Sagasti et al., 1999). The mutation of *lim-4* causes the AWB neuron to adopt the fate of the AWC neuron; consequently, AWB fails to mediate repulsive behavioral responses to appropriate environmental stimuli and to instead mediate attractive responses,, as does the AWC neuron (Sagasti et al., 1999). While these three homeobox-containing genes have clear roles in thermosensory functioning, they play important and overlapping roles in other *C. elegans* development processes.

### 1.2 The structure and roles of *lin-11* in *C. elegans*

In addition to its role in neuronal differentiation, *lin-11* is also required in the development of vulva precursor cells (VPC) and the vulva-uterine connection (Gupta et al., 2002; Hobert et al., 1998; Newman et al., 1999; Sarafi-Reinach et al., 2001). During early L3 vulva development, *lin-11* is required to produce the correct patterning of vulva invagination; during this stage high *lin-11::GFP* expression is seen in vulC and vulD precursor cells (Gupta et al., 2003). However, during mid-L4, *lin-11::GFP* expression is observed in all vulva cells (Gupta et al., 2003). In addition, *lin-11* is required for uterine

morphogenesis (Gupta et al., 2002; Newman et al., 1999). In *lin-11* mutants the uterine seam cells (utse) are missing; thus, in these mutants the utse fails to fuse with the anchor cell and as a result a functional uterine-vulva connection is not made. This detrimental development phenotype leads to the animals' eggs being unable to leave the uterus and for the progeny to hatch internally, resulting in a "bags of worms" (Horvitz and Sulston, 1980; Newman et al., 1996; Newman et al., 1999).

### 1.3 The role of *lin-11* in the egg-laying system

*lin-11* plays multiple roles in the formation of the vulva and the vulva-uterine connection. Vulva development begins when neuro-ectoblast cells divide and give rise to twenty-four cells. The twelve anterior cells give rise to the ventral cord neurons while the twelve posterior hypodermal cells give rise to the vulva precursor cells (VPC) (Sulston and Horvitz, 1977). Six of the twelve hypodermal cells – P3.p, P4.p, P5.p, P6.p, P7.p and P8.p – acquire $1^o$, $2^o$, or $3^o$ fates, depending on the intensity of the inductive signals each cell receives from the anchor cell (AC), which is located in the gonad, as illustrated in Figure 4 and 5 (Sulston and Horvitz, 1977; Paul and Horvitz, 1991). The VPC fates are acquired in a specific and invariant pattern: $3^o$-$3^o$-$2^o$-$1^o$-$2^o$-$3^o$; this corresponds to P(3-8).p (Sternberg, 2005). The cell closest to the AC acquires the $1^o$ fate, leading to three divisions, producing eight daughter cells that then become two pairs of the vulE and two pairs of the vulF precursor cells (Figure 3) (Kirouac and Sternberg, 2003). The two adjacent VPCs acquire the $2^o$ fate, with each giving rise to seven daughter cells each that

then each give rise to vulB1, vulB2, vulD and pairs of vulA and vulC precursor cells (Kirouac and Sternberg, 2003; Sharma-Kishore et al., 1999). Finally, $3^{o}$ cells divide once before the daughter cells fuse with the hypodermal syncytium, known as hyp7 (Sternberg and Horvitz, 1991; Sharma-Kishore et al., 1999). vulF connects directly with the uterine cell uv1; vulE facilitates structural attachments to the lateral hypodermal seam cells; vulC and vulD attach to the vulval muscle that opens the vulva for the passage of eggs; and vulA attaches to hyp7 (Chang et al., 1999; Newman et al., 1999). Once the AC invades the vulval epithelium, the adult vulval cells fuse with their corresponding partners and form seven toroidal rings, spurring the development of the vulva organ (Sherwoord and Sternberg, 2003; Sternberg, 2005).

In wildtype, the two vulva precursor cells are determined to undergo an asymmetrical division of opposite polarity: P5.p undergoes a lineage LLTN (L-longitudinal, T- transverse, N-no division) and P7.p undergoes NTLL division, as shown in Figure 3. In *lin-11* mutants, the NT portion of $2^{o}$ cells undergoes a symmetric, as opposed to an asymmetric, cell division (Ferguson et al., 1987). Thus, these animals adapt LLLL cell lineage rather than a NTLL pattern (Ferguson et al., 1987). Using cell specific fate markers like *zmp-1*, *egl-17, ceh-2* and *cdh-3* in wildtype animals, it has been shown that the function of *lin-11* is required for cell fate specification in vulA, vulB1, vulB2, vulC, vulD, vulE, and VulF (Gupta et al., 2003; Inoue et al., 2004). However, in *lin-11* mutants, vulC and vulD cells (2° lineage) and vulE and vulF cells (1° lineage) do not differentiate (Gupta et al., 2003). Thus, the defects in vulval cell marker expression found

in *lin-11* mutant animals illustrate that *lin-11* is required in the specification of both 1° and 2° lineage cells.

In the adult hermaphrodite, the egg is fertilized in the spermatheca and passed into the uterus, before being laid through the vulva as a result of contraction achieved via specialized uterine and vulval muscles (Newman et al., 1995). The connection between the uterus and vulva forms when three ventral uterine precursor cells (VU) in the gonad divide twice, giving rise to twelve cells during the L3 stage (Kimble and Hirsh, 1979; Newman et al., 1996); six of these precursor cells divide to become π cells that are located closer to the AC, while the other six cells become ρ cells (Newman et al., 1995). The decision as to what becomes a π cell and what becomes a ρ cell is made by the AC via LAG-2 and LIN-12-mediated lateral signaling, which gives rise to π cells as illustrated in Figure 4(Newman et al., 1995). The π cells undergo one round of division and produce utse and uv1 cells, whereas the ρ cells divide twice and generate cells that have neither the utse nor the uv1 fate (Newman et al., 1996). Eight of the π progeny fuse with each other to form a large multinucleated utse; the remaining four form adherens junctions with the vulF, thus becoming uv1 cells (Chang et al., 1999; Newman et al., 1996). The AC then fuses with the utse syncytium, resulting in a flat H-shaped multinucleated cell (Newman et al., 1996). A thin layer of the utse syncytium is present above the vulva until the adult stage, in which the uterus is connected to the vulva; however, this thin layer may be broken down by the passage of the first embryo (Chang et al., 1999; Newman et al., 1996).

The formation of vulval-uterine connections is required for the expulsion of the eggs and for successful copulation. The π cell fate requires the function of the *lin-12* gene, as shown by Newman and colleagues (1999); both the loss of π cell fates and the gain of extra π cell fates are specified by *lin-12* receptor mutation (Newman et al., 1999). LIN-12 activation in a VU causes the daughter cells to acquire the π fate. The π cells express *lin-11*, giving rise to utse (Newman et al., 1995, 1999). This suggests that the *lin-12* receptor gene is upstream and that activation of this receptor causes the expression of *lin-11* in π cells. Furthermore, the function of *lin-11* is only important in the differentiation of π progeny, and not in the asymmetric cell division of π cells (Newman et al., 1999). *lin-11* function is required for the proper migration of π progeny nuclei and the AC. Thus, in wildtype animals, the π cell migrates distally from the center of the uterus; in *lin-11* mutants, however, both the π cell and the AC nucleus fail to move from their positions, and thus fail to fuse. Instead, in *lin-11* mutants the π cells are scattered around and the AC becomes larger and bloated, the latter being a common attribute of animals lacking π cells (Newman et al., 1999). In addition, there are many other genes that have been shown to be required for the proper differentiation of utse, including *egl-38, egl-13 (cog-2), lag-1* and *smo-1* (Broday et al., 2004; Chamberlin et al., 1997; Cinar et al., 2003; Hanna-Rose and Han, 1999; Gupta et al., 2002).

The expression of *lin-11* is also important to the proper function of several neurons, specifically: thirteen head neurons and four tail neurons, as shown in Table 1; these neurons fall under different classes, including: chemosensory, odorosensory, and

interneurons. The role of these neurons will be discussed in detail in a later section.

### 1.4 The role of *lin-11* in neuronal differentiation

*lin-11* is essential to the proper differentiation and function of olfactory (AWA), thermosensory (AIZ) and chemosensory (ASG) neurons; but it is not essential to the generation of these neurons (Cassata et al., 2000; Hobert et a., 1998; Sarafi-Reinach et al., 2001). The role of *lin-11* in the differentiation and function of AWA, AIZ and ASG neurons is discussed below.

*C. elegans* sense chemicals in their environment using a small number of well-characterized chemosensory neurons. In total, there are 11 pairs of chemosensory neurons; they have been identified by laser ablation studies that also reveal that each neuron type responds to a distinct but partially overlapping set of chemicals (Bargmann and Mori, 1997). Volatile odorants are sensed by bilaterally symmetrical AWA, AWB and AWC olfactory neurons (Bargmann et al., 1993). Aqueous attractants are sensed by ASE neurons, while pheromones are sensed by ADF, ASI, ASG and ASJ neurons (Bargmann and Horvitz, 1991). *lin-11* expression was shown to be important in ADF, AWA, and ASG neurons (Cassata et al., 2000; Hobert et al., 1998; Sarafi-Reinach et al., 2001). Specifically, the *odr-7* gene encodes a nuclear hormone receptor that has been shown to be required for the proper function of the AWA neuron (Sarafi-Reinach et al., 2001; Sengupta et al., 1994). However, in *lin-11* mutants the expression of *odr-7* is altered, which suggests that *lin-11* expression is required to initiate *odr-7* expression in

AWA neurons. These animals lack AWA neurons and fail to respond to the volatile odorant chemical diacetyl and pyrazine (Segupta et al., 1994). The ASG neuron is a lineal sister of the AWA neuron, and *lin-11* expression is required for the proper function of the *unc-30* gene in the ASG neuron; the *unc-30* gene encodes a Ptx family transcription factor (Jorgensen, 2005). Furthermore, it is known that *lin-11* is required for the proper function of the ADF neuron and it has been shown that the ADF neuron has a minor role, in combination with the ASC and ASI amphid neurons, in detecting biotin, $Cl^-$, $Na^+$ and cAMP in the environment (Bargmann & Horvitz, 1991a). The ADF neuron is required for dauer formation because it senses food or pheromone signals (or both) from the environment; this same neuron then regulates the animal's developmental transition, causing it to either continue growing or to enter the low metabolic dauer stage (Bargmann and Horvitz, 1991b). However, the reason(s) that *lin-11* spatial and temporal expression is required by the ADF neuron is unknown.

Thermosensation in *C. elegans* requires the proper function of three pairs of neurons: AFD, AIY and AIZ (Cassata et al., 2000). *C. elegans* has a limited physiological temperature range – ~ $12^oC$ - $26^oC$ – in which it can achieve healthy metabolic function and fertility (Cassata et al., 2000). *lin-11* function is required only in the AIZ interneuron (Cassata et al., 2000; Hobert et al., 1998). Laser ablation studies have shown that killing AIZ neurons causes wildtype animals to adopt a thermophilic trait, which is also characteristic of *lin-11* null mutant animals (Hobert et al., 1998). It has been suggested that *C. elegans'* thermosensation output occurs between two balanced, but opposite

sources of inputs, regulated, respectively, by AIY and AIZ neurons (Hobert et al., 1998; Mori and Ohshma, 1995).

### 1.5 AVG as a pioneering neuron and role of *lin-11* in AVG differentiation

Many other neurons require the proper function of *lin-11,* as illustrated in Table 1, including AVG. The AVG's cell body is located in the retrovesicular ganglion, at the anterior end of the ventral cord. AVG is a pioneer neuron that identifies the ventral cord axon tract (Durbin, PhD thesis University of Cambridge, 1987). In order for the AVG growth cone to reach its proper destination, it must be guided by multiple UNC-6/netrin cues, which are located in their extracellular environment during ventral cord development (Wadsworth and Hedgecock, 1996). The first UNC-6/netrin cue acts globally and peaks near the ventral midline of the AVG's body wall, acting as an attractive cue for the AVG neuron; thus, it allows the AVG to cross the midline body (Wadsworth and Hedgecock, 1996). A second UNC-6/netrin cue, produced by AVG and restricted to the anterior and posterior of the animal, allows other neurons, like RIF, to migrate using the AVG axon projection as guidance (Wadsworth and Hedgecock, 1996). A third netrin cue, specific to pioneer neurons, AVG, provides them with pathways into the ventral cord (Wadsworth and Hedgecock, 1996). Laser ablation studies have shown that killing AVG pioneer neurons causes disorganization in ventral cord axon bundles, which as a result split into distinct sub-bundles, with the axons occasionally crossing the midline and entering the left tract (Durbin, PhD thesis University of Cambridge, 1987).

Axonal disorganization is seen more prominently in certain classes of neurons, especially interneurons and D-type motor neurons (Durbin, PhD thesis University of Cambridge, 1987). Thus, Durban speculated that although AVG is a pioneer neuron, it is not essential to the normal outgrowth of other axons in the right axon tract, which must receive other cues from their environment to ensure proper navigation (Durbin, PhD thesis University of Cambridge, 1987).

*lin-11* plays an important role in the generation of AVG. Although it does not control the birth of the presumptive AVG but it is necessary for AVG differentiation. In *lin-11* mutants AVG fails to form based on the absence of expressions of two AVG-specific molecular markers *glr-1::GFP* and *odr-2::GFP* (Hutter, 2003; Hutter et al., 2005).

### 1.6 Aim of the thesis

The aim of this thesis is to dissect the molecular mechanism of *lin-11* function in neuronal cell differentiation. To that end, I have carried out two complementary sets of experiments. One of these focuses on the transcriptional regulation of *lin-11* in amphid sensory neurons during the mediating of responses to olfactory, chemosensory and thermosensory stimuli. The other concerns the requirements of *lin-11* protein domains.

### 1.7 Major Findings

In the past, three undergraduate students in the Gupta lab (Asad Siddiqi, Alem Adatia and Carly Ching) examined the enhancer activities of the two largest *lin-11* introns: 3 (1355bp) and 7 (1284bp). They found that while intron 7 is expressed in AVG and another neurons located between the isthmus and the terminal bulb of the animal, intron 3 expression is found in ten ventral cord neurons, including AVG. Similar neuronal expression patterns were also observed in the corresponding *C. briggsae lin-11* enhancers. These results suggest that the function of *lin-11* is conserved between these two closely related species.

I have sequenced eleven *lin-11* mutant alleles to determine the nature of the mutation and I have observed the vulva morphology in these mutant alleles. Using GFP and CFP molecular markers, I was able to analyze amphid sensory neurons in the ventral cord of worms with the *lin-11* null allele n389, or with the weaker allele, ps1. I also used similar markers to analyze vulva cell morphology in *lin-11* null mutants. My results show that *lin-11* expression is necessary for the proper function of amphid neurons, including AVG. In addition, rescue experiments using pGF50, which contains the entire *lin-11* genomic DNA sequence, were able to rescue both the AVG neuron and the egg-laying defect in *lin-11* mutants in order to use them as a control. However, the pGLC70 plasmid, which contains the intron 7 enhancer that drives the expression of exon 8, 9, and 10 of *lin-11* cDNA, was unable to rescue the *lin-11* phenotypes, suggesting that the proper function of LIN-11 protein is required in order to rescue the *lin-11* phenotypes.

Next, I searched for transcription factors (TF) that might regulate the expression of lin-11 in an AVG neuron. This was done using a bioinformatics program, MatInspector (http://www.genomatix.de/). The list of TFs with a potentially regulatory role in the AVG expression of *lin-11* allowed me to test their in vivo role using an RNA interference (RNAi) approach. For this, I used a neuronal hypersensitive strain, *eri-1; lin-15b*. Two families of TFs, Erythroid-Like Transcription factor family (elt) and Doublesex/MAB-3 Domain family (dmd), showed reduced AVG expression. Further examination of the *elt* and *dmd* genes in *lin-11* regulation should to provide important information about their mechanism of action in AVG differentiation.

The sequence analysis of *lin-11* mutant alleles demonstrated various types of mutations affecting, in addition to the proline rich region, both the Hox and HD domains, which have a very important role in neuronal and vulva development. Mutations that affect these conserved regions of *lin-11* result in very sever phenotypes, such as protruding vulvas, egg-laying defects, locomotion defects and many others; these will be discussed further in more detail.

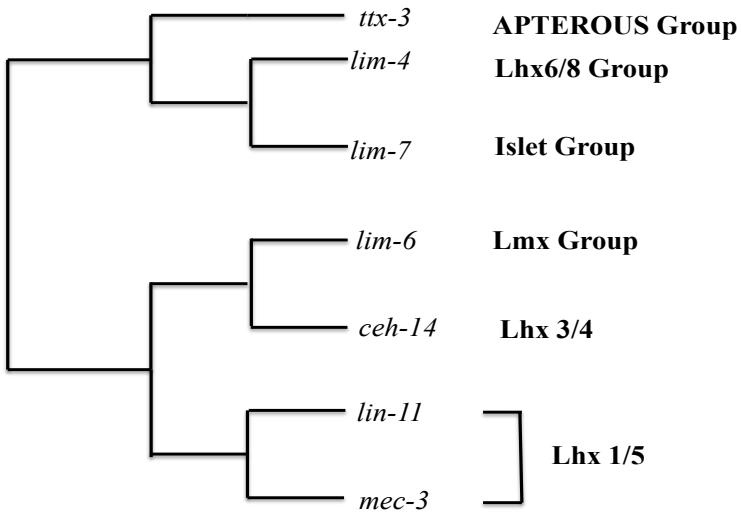


**Figure 1- Phylogenetic relationship of *C. elegan* LIM-HD proteins.** Adapted from Hobert and Westphal, 2000.

A)


—C-$x_2$-C—$x_{17-19}$-H-$x_2$-C-$x_2$-C-$x_2$-C-$x_{7-11}$-(C)$x_8$-C → LIM Domain

B)

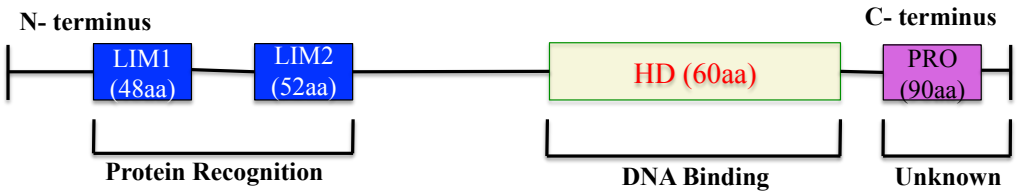


**Figure 2- LIN-11 molecular characteristics**

A) List of LIN-11 amino acids (aa). Underlined aa indicate the LIM1 and LIM2 beginning and end sites. Red colour aa's showing the conserved cysteins in the LIM domains. Blue coloured amino acids represent the HD, and the purple coloured proline represents the proline region of LIN-11. B) Schematic structure of LIN-11 protein.

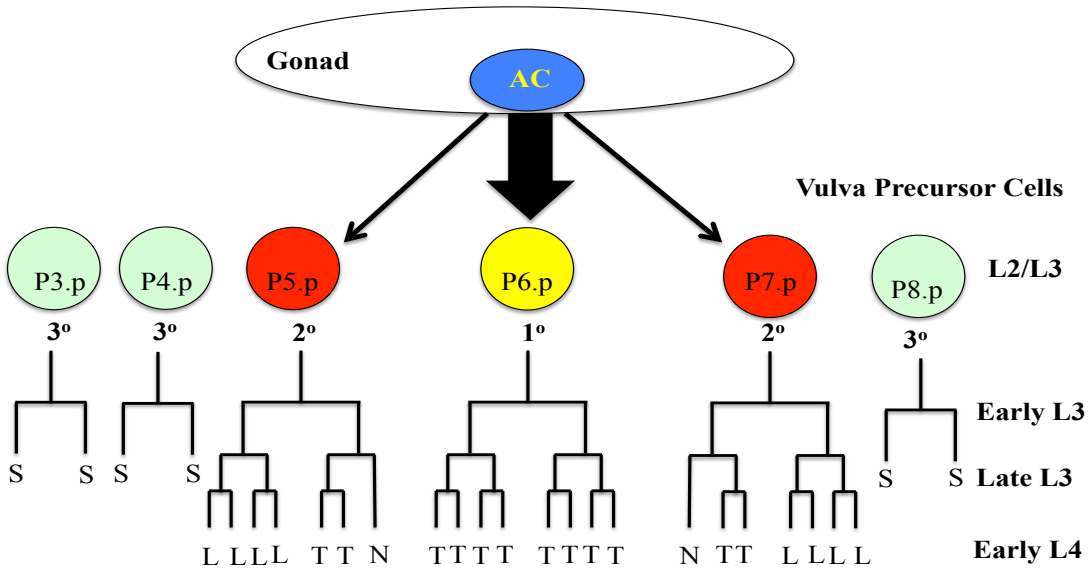


**Figure 3- Vulva development in wildtype animals.**

During L2/L3 stages, signal from the anchor cell (AC) induces P5.p, P6.p and P7.p VPCs to adopt vulval $1^{o}$ and $2^{o}$ cell fates. $1^{o}$ cell give rise to the TTTT terminal cell division axes, while $2^{o}$ cell give rise to NTLL terminal cell division axis (N, no division; T, transverse; L, longitudinal). During early L4 stage Pn.pxxx cell invaginate and form the vulva opening. Adapted from (Gupta et al., 2003).

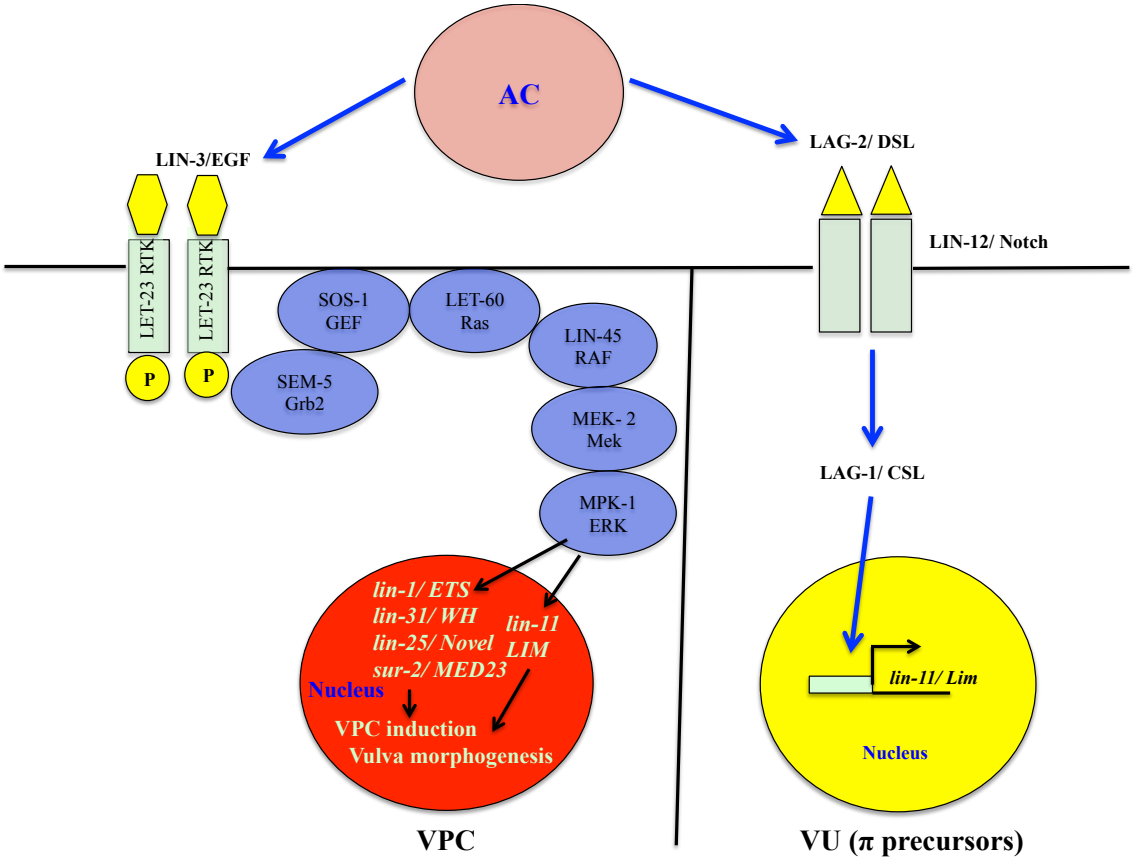


**Figure 4- The RTK/Ras/MPK signaling pathways and π precursors cell signaling pathway activation by AC cell in the gonad.**

LIN-3 binds to the receptor tyrosine kinase, LET-23, which causes RTK to cause dimerization and autophosphorylation. This will cause the activation of adapter protein SEM-5 and SOS-1which activates LET-60/Ras; LET-60 will activate LIN-45/Mek. Activated MEK-2 activates the MAP Kinase, MPK-1/Erk. MPK-1 will move to the nucleus and to promote the transcription of *lin-1* gene. Adapted from (Sundaram M. V. 2006). In order for VU cells to acquire π fate not ρ, AC cell signals *lin-12* receptor via *lag-2* to activate the expression of *lin-11* in these cells.

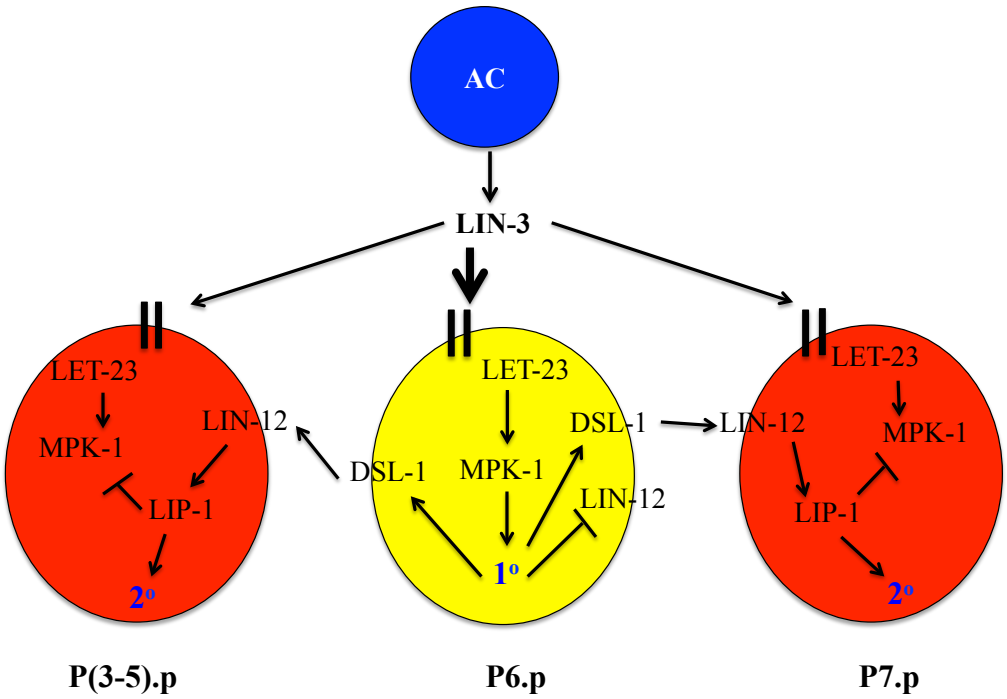


**Figure 5- WNT, Ras and Notch Pathways in VPC fate specification.**

Thin long arrow represents low levels of LIN-3 from AC binding to the LET-23 receptor, and causes low level of MPK-1 pathway to be activated. However, LIN-12 receptors are activated by DSL-1 in P(3-5).p and P7.p which will these cells to acquire $2^{o}$ fate.

**Table 1-** List of head and tail neurons that require the function of *lin-11* (WormAtlas, V 1.0).

| Neuron Name | Neuron Type | Function |
|---|---|---|
| | | **Head Neurons** |
| AVA | Interneuron | Backward locomotion |
| AVE | Interneuron | Backward locomotion |
| ADF | Sensory | Dauer Entry<br>Environmental stimulie detection: O2, cAMP, biotin, Cl- and Na+ |
| ASH | Sensory | Touch avoidance response<br>Environmental repulsive cue detection: Cd++, Cu++, protons, alkaloids, and detergents. |
| ADL | Sensory | Heavy chemicals like Cd++ and Cu++<br>Social feeding behavior |
| AWA | Odorosensory | Chemotaxis to diacetyl, pyrazine, trimethylthiozole |
| ASG | Chemosensory | Chemotaxis to lysine. cAMP, biotin, $Cl^-$, and $Na^-$<br>Control entry to dauer stage |
| RIC | Interneuron | Not Known |
| AIZ | Interneuron | Thermosensation |
| AVG | Interneuron | Pioneer the right tract of the ventral nerve cord |
| AIY | Interneuron | Thermosensation |
| AVH | Interneuron | Not Known |
| AVJ | Interneuron | Not Known |
| | | **Tail Neurons** |
| PVP | Interneuron | Pioneer the left side of the ventral cord |
| PVQ | Interneuron | Pioneer the left side of the ventral cord |
| DVA | Interneuron | Touch inputs to anterior and posterior<br>Stretch receptor that regulates sensory-motor integration during locomotion |
| DVC | Interneuron | Not Known |

# Chapter 2- Materials and Methods

## 2.1 Strains and General Methods

Culturing and genetic manipulations of *C. elegans* have been previously described (Brenner, 1974). All experiments were completed at 22$^{o}$C unless otherwise noted. Neuronal cell body position and axonal projector is described in Wormatlas (www.wormatlas.org). The strains used in this study are listed in Table 2.

## 2.2 Genetic Cross

Genetic crosses required to obtain GFP reporter expressing in *rrf-3; eri-1* hypersensitive mutant background in order to perform RNAi experiment in the neurons, this was accomplished by crossing 8-10 *bhEx*95 males which carry the full intron 7 sequence and 2-4 *rrf-3* hermaphrodites on agar plates. Animals were allowed to mate for 3-4 days to produce F1 heterozygous fluorescent male. The F1 heterozygous fluorescent males were selected and crossed to 3-4 *eri-1* mutant hermaphrodites, and 6 hermaphrodite animals were cloned out in different agar plates and were allowed to self-fertilize. And PCR was used to determine which plates out of these 6 are heterozygous for both mutations; from the heterozygous plate 48 F2 hermaphrodites were cloned out, this time to identify homozygous double mutants (Figure 6). Genomic DNA was extracted from single worms to perform PCR in order to determine which agar plates contain heterozygous mixture. Two sets of primers were designed to amplify the *rrf-3* (pk1426)

which has a 3.0 kb deletion and *eri-1* (mg366) which has 23 bp insertion mutations. Using primers GL569/GL570 in wildtype animals 3.6 kb DNA fragment size will be amplified by PCR, however, in *rrf-3* mutants only 0.6 kb DNA fragment size will be amplified; but in heterozygote animals both 3.6 kb and 0.6 kb DNA bands will be present on the agrose gel. The plate of worms that had both 3.6 kb and 0.6 kb DNA fragments were allowed to self fertilize and 48 worms were cloned out into different plates. Once again using PCR to determine which plates contains the homozygote animals for both mutations. As illustrated in Figure 7, the double hypersensitive mutant showed only one bright DNA fragment band at 0.6 kb to suggest that this strain is homozygote for *rrf-3* mutation. Similarly, in order to determine homozygote *eri-1* animals one pair of primer was also designed, GL571/GL573, to amplify 150 bp in wildtype animals and 173 bp in homozygote *eri-1* mutant animals (Figure 7). Using *eri-1* primer set 173 bp DNA fragment was amplified for the double mutant, DY387, to suggest this mutant is also homozygous for *eri-1* mutation (Figure 7).

**P** *rrf-3/rrf-3* x *bhEx*95♂

↓

**F1** *rrf-3*/+ (GFP)♂ x *eri-1/eri-1*

↓

**F2** *rrf-3*/+; *eri-1*/+; GFP → 50%

+/+; *eri-1*/+; GFP → 50 %

↓

**F3** *rrf-3/rrf-3*; *eri-1/eri-1;* GFP → 1/16 chance (clone 48 plates)

**Figure 6- Schematic diagram illustrating the genetic cross**

This genetic cross was used to obtain a hypersensitive RNAi strain, *eri-1; rrf-3*; GFP in order to perform RNAi in the AVG neurons.

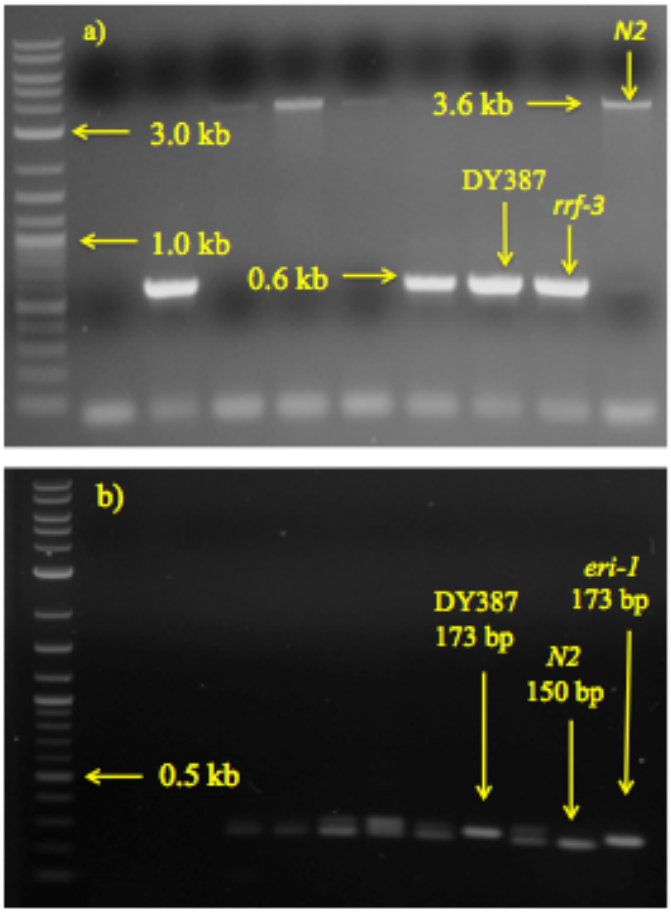


**Figure 7- PCR validation for the genetic cross for double homozygous mutants.**

a) Illustrating PCR amplified *rrf-3* mutation fragment size. Using GL569/GL570 primer set to amplify 3.6 kb band size in wildtype animals and 0.6 kb band size in *rrf-3* homozygous mutant animals. In addition, the double mutant strain, DY387, also show 0.6 kb band size as well, to suggest that DY387 is homozygote for *rrf-3* mutation. b) PCR amplified *eri-1* mutation. Using GL571/GL573 primer set to amplify 150 bp fragments in wildtype animals and 173 bp in *eri-1* homozygous mutant. As illustrated in b) the DY387 double mutant is also showing 173 bp DNA amplified fragment size similar to that of *eri-1* fragment, to suggest that this strain is homozygous for *eri-1* mutation as well.

## 2.3 Generation of Transgenic Strains

The transgenic lines were generated using standard microinjection technique (Mello et al., 1991) using *C. elegan unc-119* (Maduro and Pilgrim, 1995). The concentration of each plasmid injected is shown in the Table 2.

## 2.4 Heat-shock Protocol

To obtain a high incidence of male culture in *bhEx*95 animals in order to set up genetic cross; four plates of agar and each plate containing twenty late L4 hermaphrodite animals were heat shocked at 31$^{o}$C for 6 hours, and during the F1 generation the male animals were selected.

## 2.5 Microscopy

Worms were mounted on agar pads using M9 buffer and sodium azide. Different stages of the animals were examined under Nomarski optics using Zeiss Axioimager D1 and Nikon Exlipse 80i. For GFP reporter expressing strains, epifluorescence was visualized by using Zeiss Axioimager D1 microscopeequipped with the GFP filter HQ485LP (Chroma Technology). The confocal images were taken on a Leica DMI 6000 B laser-scanning microscope using a Leica TCS-SP5 scanner and Leica Application Suite Advanced software.

## 2.6 Vulval phenotype and neuronal cell analysis

Vulva morphology was scored using wildtype N2 vulva as a standard. We scored vulva phenotype during late L4 stages of development. We used two criteria to rank *lin-11* mutant alleles: 1) utse morphology and vulva morphology, which is further broken down to finger protrusions and proper invagination. If animals were deformed in one of the categories were ranked as weak allele, two categories were considered as intermediate allele, and if they were defective in all categories were ranked as strong allele.

Neuronal cell analysis were conducted by using cell body position and axonal projection as reference point in wildtype animals to identify if the same neurons were present in mutant alleles. We used neuronal marker odr-2::CFP to visualize all the amphid sensory neurons in wildtype and *lin-11* mutants, and we used Wormatlas (www.wormatlas.org) to identify these neurons.

## 2.7 Molecular Biology

All the primers that used in this study are listed in Table 3 and their molecular position is shown in (Figure 7). Five plasmids were made for this study, and for each plasmid detailed molecular structure is provided (Figure 8-12).

### 2.7.1 pGLC83

To construct *egl-17::CFP,* 158 bp fragments were amplified by PCR using primers GL705 and GL706. The PCR products were digested with *SphI* and *XbaI* and subcloned into pGLC25 plasmid. pGLC25 plasmid is 5.3 kb in size and it contains Δpes10 promoter and Fire vector pPD 136.61 (Fire lab vector, *www.addgene.com)*. For confirmation SphI and KpnI restriction enzymes were and finally the fragment sizes were confirmed by gel electrophoresis.

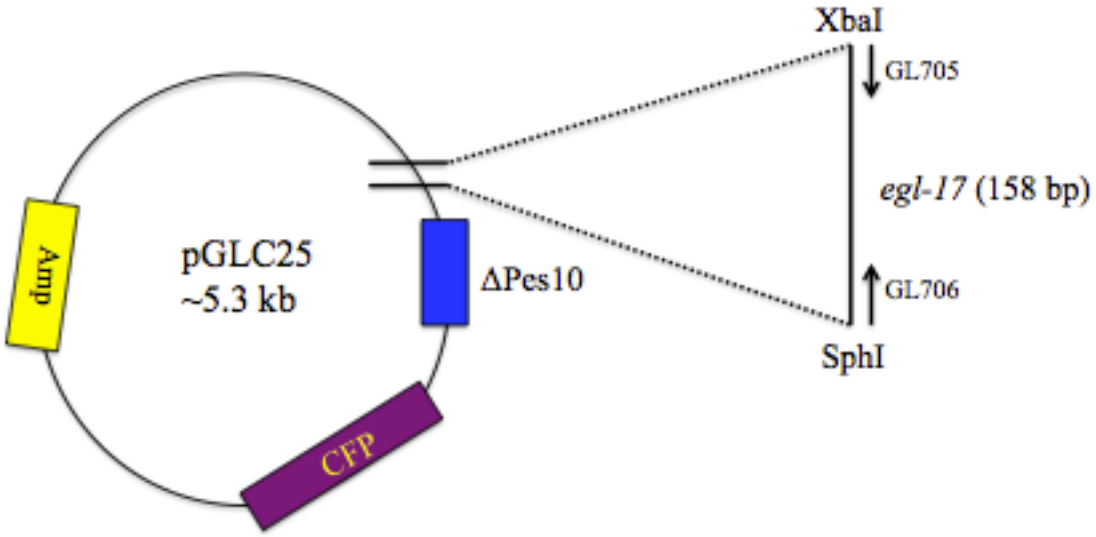


**Figure 8-** Molecular structure of pGLC83 plasmid.

### 2.7.2 pGLC84

To construct *egl-17::YFP,* 158 bp fragments were amplified by PCR using primers GL705 and GL706. The PCR products were digested with *SphI* and *XbaI* and subcloned into pGLC24 plasmid. pGLC24 plasmid is 5.4 kb in size and it contains Δpes10 promoter and Fire vector pPD 136.61 (Fire lab vector, *www.addgene.com)*. For confirmation SphI and KpnI restriction enzymes were and finally the fragment sizes were confirmed by gel electrophoresis.

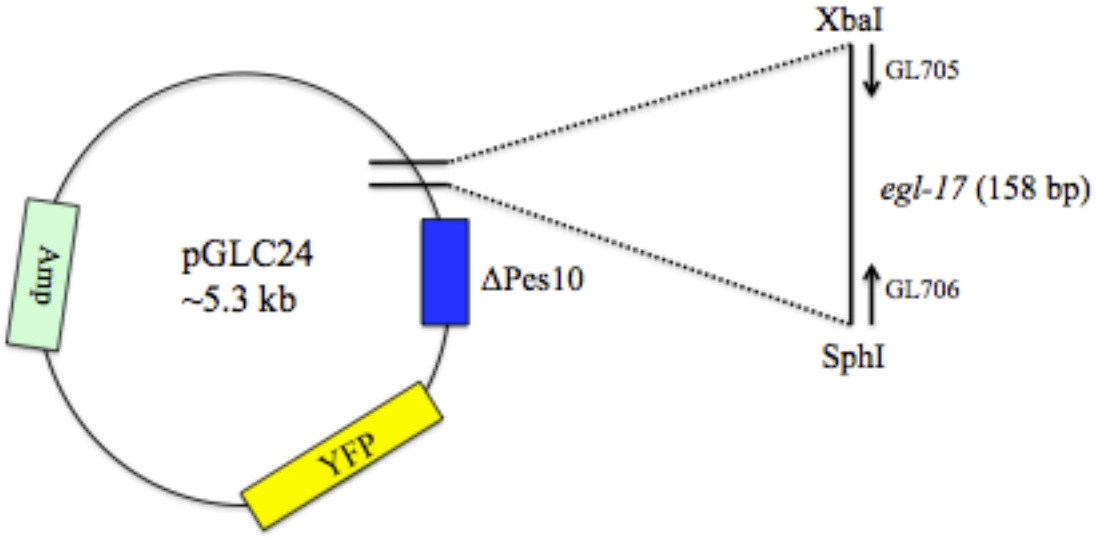


**Figure 9-** Molecular structure of pGLC84 plasmid.

### 2.7.3 pGLC85

To construct *zmp-1::CFP,* 386 bp fragments were amplified by PCR using primers GL707 and GL708. The PCR products were digested with *SphI* and *XbaI* and subcloned into pGLC25 plasmid. pGLC25 plasmid is 5.3 kb in size and it contains Δpes10 promoter and Fire vector pPD 136.61 (Fire lab vector, *www.addgene.com)*. For confirmation SphI and KpnI restriction enzymes were and finally the fragment sizes were confirmed by gel electrophoresis.

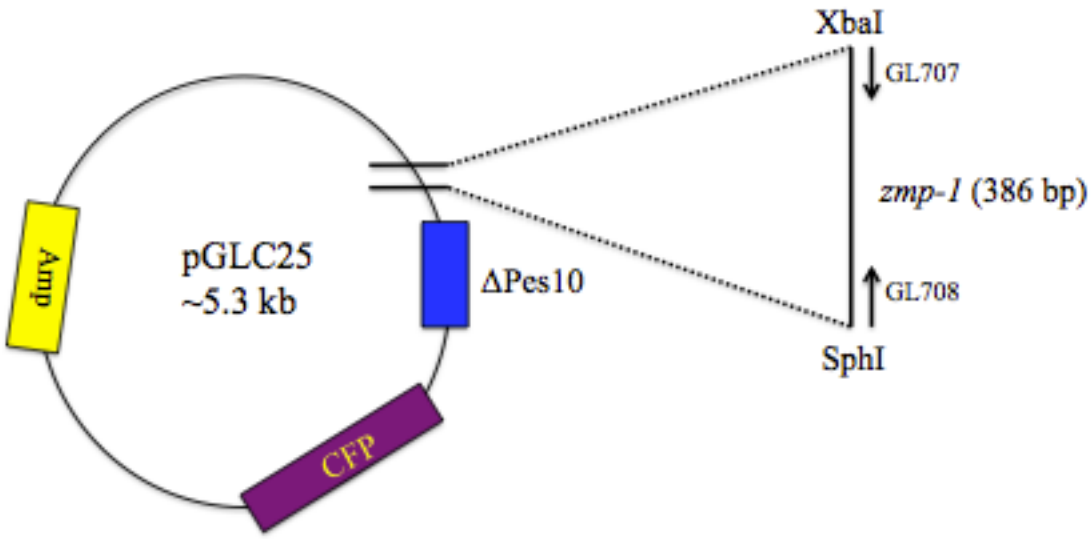


**Figure 10-** Molecular structure of pGLC85 plasmid.

### 2.7.4 pGLC86

To construct *zmp-1::YFP,* 386 bp fragments were amplified by PCR using primers GL707 and GL708. The PCR products were digested with *SphI* and *XbaI* and subcloned into pGLC24 plasmid. pGLC24 plasmid is 5.3 kb in size and it contains Δpes10 promoter and Fire vector pPD 136.61 (Fire lab vector, *www.addgene.com)*. For confirmation SphI and KpnI restriction enzymes were and finally the fragment sizes were confirmed by gel electrophoresis.

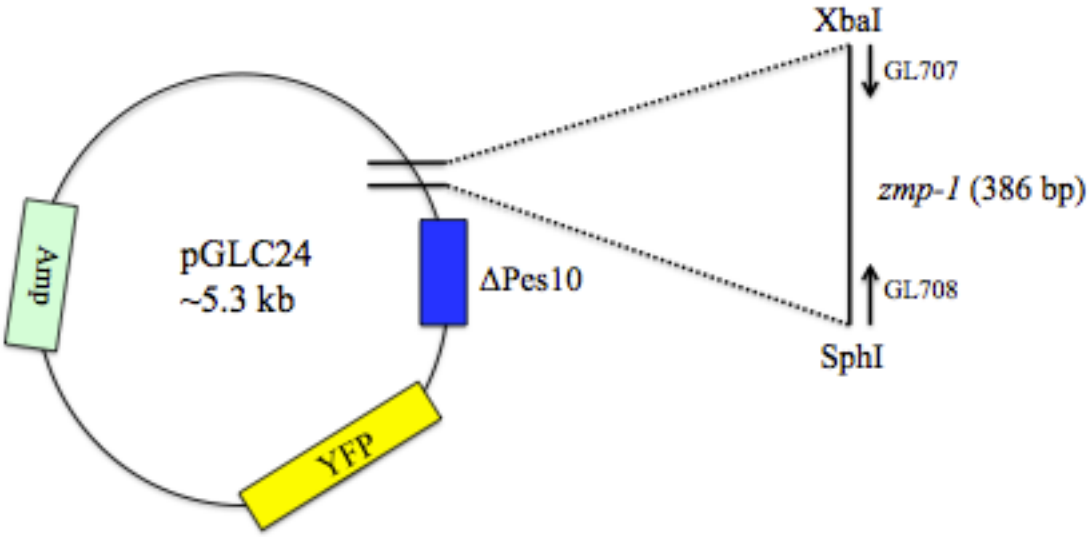


**Figure 11-** Molecular structure of pGLC86 plasmid.

### 2.7.5 pGLC87

Plasmid pYK452F7-1 was digested with SpeI and SphI and 3.1 kb *lin-11* cDNA sequence was gel purified and ligated into pGLC67. pGLC67 plasmid contains intron 7 enhancer, thus, the full cDNA of *lin-11* is inserted downstream of intron 7.

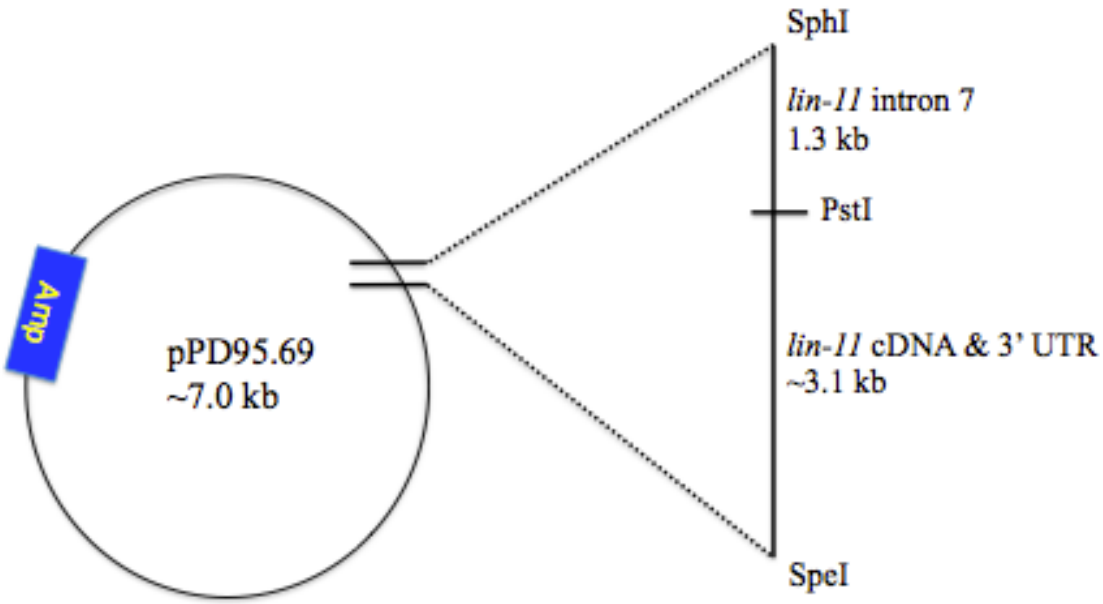


**Figure 12-** Molecular structure of pGLC87 plasmid.

## 2.8 RNAi

RNAi was performed on agar plates containing 0.6% Na2HPO4, 0.3% KH2PO4, 0.1% NH4Cl, 0.5% Casamino Acids, 2% Agar, 1mM CaCl2, 1mM MgSO4, 0.0005% cholesterol, 0.2% β-lactose, and 50 μg/ml Carbenicillin. Plates were seeded with 150 μl of overnight grown HT115 bacterial culture in LB and Carbenicillin media that produces dsRNA of the gene of interest. Eight to 10 L4 stage worms were placed on RNAi plates and the AVG neuron of F1 progeny were examined. For those genes that caused lethality or embryo arrest, animals were subjected to RNAi treatment during the L1 larval stage. All RNAi experiments were repeated at least 3-4 times and batches that produces consistent results were analyzed.

### 2.9 Electrotactic assay

Worms were grown at 20°C on standard NG agar plates containing *E. coli* OP50 culture as previously described (Brenner, 1974). Synchronized worms were used for all the assays and were prepared by bleach treatment (Rezai et al., 2010). Gravid hermaphrodites were treated with a bleach solution (commercial bleach: 4N NaOH in a 3:2 ratio) and embryos were incubated in M9 buffer (0.02M $KH_2PO_4$, 0.04M $Na_2HPO_4$, 0.086M NaCl and 1 ml of 1M $MgSO_4$ in a final volume of 1 liter) at room temperature for 48 hours to obtain a synchronized population of arrested L1 animals. After bleach treatment, the *lin-11*(n389) embryos were incubated in M9 buffer at room temperature for 48 hours to obtain a synchronized population of arrested L1 animals and were grown at 20°C on standard NG agar plates containing *E. coli* OP50 for 30 hours to obtain late L3 and early L4 stage animals.

| Stable Line | Plasmid | Genotype | Strain | Plasmid Concentration | Chromosome |
|---|---|---|---|---|---|
| ***C. briggsae*** | | | | | |
| bhEx137 | pGLC61 | *unc-119;* bhEx137[*unc-119*(+) + pGLC61(Cbr-*lin-11*::GFP)] | DY351 | 75 ng/ul | III; Ex |
| ***C. elegans*** | | | | | |
| bhEx95 | pGLC58 | *unc-119*(ed4); bhEx95[*unc-119*(+) + pGLC58(*lin-11*-int7::GFP)] | DY242 | 75 ng/ul | III; Ex |
| bhEx96 | pGLC59 | *unc-119*(ed4); bhEx95[unc-119(+) + pGLC59(*lin-11*-int3::GFP)] | DY243 | 75 ng/ul | III; Ex |
| bhEx97 | pGLC59 | *unc-119*(ed4); bhEx97[unc-119(+) + pGLC59(*lin-11*-int3::GFP)] | DY244 | 75 ng/ul | III; Ex |
| bhEx98 | pGLC59 | *unc-119*(ed4); bhEx98[*unc-119*(+) + pGLC59(*lin-11*-int3::GFP)] | DY245 | 75 ng/ul | III; Ex |
| bhEx99 | pGLC58 | *unc-119*(ed4); bhEx99[*unc-119*(+) + pGLC58(*lin-11*-int7::GFP)] | DY247 | 75 ng/ul | III; Ex |
| bhEx112 | pGLC60 | *unc-119*(ed4); bhEx112[*unc-119*(+) + pGLC60(cbr-*lin-11*::GFP)] | DY296 | 75 ng/ul | III; Ex |
| bhEx113 | pGLC60 | *unc-119*(ed4); bhEx113[*unc-119*(+) + pGLC60(cbr-*lin-11*::GFP)] | DY297 | 75 ng/ ul | III; Ex |
| bhEx114 | pGLC61 | *unc-119*(ed4); bhEx115[*unc-119*(+) + pGLC60(cbr-*lin-11*::GFP)] | DY293 | 75 ng/ul | III; Ex |
| bhEx115 | pGLC60 | *unc-119*(ed4); bhEx115[unc-119(+) + pGLC60(cbr-*lin-11*::GFP)] | DY294 | 75 ng/ul | III; Ex |
| bhEx118 | pGLC67 | *unc-119*(ed4); bhEx118[*unc-119*(+) + pGLC67(*lin-11*-int7::GFP)] | DY325 | 75 ng/ul | III: Ex |
| bhEx119 | pGLC67 | *unc-119*(ed4); bhEx119[*unc-119*(+) + pGLC67(*lin-11*-int7::GFP)] | DY326 | 75 ng/ul | III; Ex |
| bhEx125 | pGLC75 | *unc-119*(ed4); bhEx125[unc-119(+) + pGLC75(*lin-11*-int7::GFP)] | DY333 | 75 ng/ul | III; Ex |
| bhEx126 | pGLC75 | unc-119(ed4); | DY334 | 75 ng/ul | III; Ex |

| | | | | | |
|---|---|---|---|---|---|
| | | bhEx125[*unc-119(+)* + pGLC75(*lin-11*-int7::GFP)] | | | |
| bhEx127 | pGLC66 | *unc-119*(ed4); bhEx127[*unc-119*(+) + pGLC66(*lin-11*-int7::GFP)] | DY335 | 75 ng/ul | III; Ex |
| bhEx128 | pGLC66 | *unc-119*(ed4); bhEx128[*unc-119*(+) + pGLC66(*lin-11*-int7::GFP)] | DY336 | 75 ng/ul | III; Ex |
| bhEx129 | pGLC65 | *unc-119*(ed4); bhEx129[*unc-119*(+) + pGLC65(*lin-11*-int7::GFP)] | DY337 | 75 ng/ul | III; Ex |
| bhEx130 | pGLC65 | *unc-119*(ed4); bhEx130[*unc-119*(+) + pGLC65(*lin-11*-int7::GFP)] | DY338 | 75 ng/ul | III; Ex |
| bhEx131 | pGLC76 | *unc-119*(ed4); bhEx131[*unc-119*(+) + pGLC65(*lin-11*-int7::GFP)] | DY339 | 75 ng/ul | III: Ex |
| bhEx136 | pGLC76 | *unc-119*(tm4063); bhEx147[*unc-119(+)* +pVH10.13(*odr-2b*::CFP)] | DY344 | 75 ng/ul | III; Ex |
| bhEx137 | pGLC61 | *unc-119*(ed4); bhEx115[*unc-119*(+) + pGLC60(cbr-*lin-11*::GFP)] | DY351 | 75 ng/ul | III; Ex |
| bhEx145 | pVH10.17 | *unc-119*(tm4063); bhEx145[*unc-119*(+) +pVH10.13(*odr-2b:*:CFP)] | DY393 | 75 ng/ul | III; Ex |
| bhEx146 | pVH10.17 | *unc-119*(tm4063); bhEx146*[unc-119*(+) +pVH10.13(*odr-2b*::CFP)] | DY394 | 75 ng/ul | III; Ex |
| bhEx147 | pVH10.17 | *unc-119*(tm4063); bhEx147[*unc-119*(+) +pVH10.13(*odr-2*b::CFP)] | DY395 | 75 ng/ul | III; Ex |
| bhEx150 | pVH10.17 | *lin-11*(n389); bhEx150 [pVH10.17(*odr-2*::CFP)] | DY400 | 75 ng/ul | I; Ex |
| bhEx157 | pGLC83<br>pGLC86<br>pVH10.17 | *lin-11*(ps1); bhEx157[pGLC86(zmp-1::YFP)+pGLC83(*egl-17*::CFP)+ pVH10.17(*odr-2b*::CFP)] | DY417 | 50 ng/ul<br>50 ng/ul<br>50 ng/ul | I; Ex |
| bhEx158 | pGLC83<br>pGLC86<br>pVH10.17 | *lin-11*(ps1); bhEx157[pGLC86(*zmp-1*::YFP)+pGLC83(*egl-17*::CFP)+ pVH10.17(*odr-2b*::CFP)] | DY418 | 50 ng/ul<br>50 ng/ul<br>50 ng/ul | I; Ex |
| bhEx159 | pGF50 | *lin-11*(n389); bhEx159 | DY423 | 10 ng/ul | I; Ex |

| | | | | | |
|---|---|---|---|---|---|
| | odr-2 | [pGF50+pVH10.17(*odr-2*::CFP)] | | 50 ng/ul | |
| bhEx160 | pGF50<br>odr-2 | *lin-11*(n389); bhEx159 [pGF50+pVH10.17(*odr-2*::CFP)] | DY424 | 10 ng/ul<br>50 ng/ul | I; Ex |
| bhEx161 | unc-119<br>pGLC86<br>pGLC83 | *unc-119*(tm4063); bhEx161[pGLC86(*zmp-1*::YFP)+pGLC83(*egl-17*::CFP)] | DY425 | 50 ng/ul<br>50 ng/ul<br>50 ng/ul | I; Ex |
| bhEx162 | *unc-119*<br>pGLC86<br>pGLC83 | *unc-119*(tm4063); bhEx162[pGLC86(*zmp-1*::YFP)+pGLC83(*egl-17*::CFP)] | DY426 | 50 ng/ul<br>50 ng/ul<br>50 ng/ul | I; Ex |
| bhEx163 | *odr-2*<br>pGLC70 | *lin-11*(ps1); bhEx163 [pGLC70+pVH10.17(odr-2::CFP)] | DY428 | 50 ng/ul<br>10 ng/ul | I; Ex |
| bhEx164 | *odr-2*<br>pGLC70 | *lin-11*(ps1); bhEx164 [pGLC70+pVH10.17(*odr-2*::CFP)] | DY429 | 50 ng/ul<br>10 ng/ul | I; Ex |
| _ | pGLC58 | *eri-1*(mg366)IV; *lin-15b*(n744)X; pGLC58 | DY405 | 75 ng/ul | IV; X; Ex |
| _ | pGLC59 | *eri-1*(mg366)IV; *lin-15b*(n744)X; pGLC59 | DY406 | 75 ng/ul | IV; X; Ex |
| _ | pGLC58 | *rrf-3*(pk1426); *eri-1*(mg366); bhEx95[unc-119(+) + pGLC58(*lin-11*::GFP)] | DY387 | _ | II; IV; ex |

**Table 2-** List of transgenic strains that are used in this study and plasmid concentration that were microinjected to obtain the transgenic animal(s).

| Allele | Strain | Source |
|---|---|---|
| n389 | PS2821 | Paul Sternberg Lab |
| n382 | MT382 | CGC |
| n672 | MT1307 | CGC |
| n1281 | MT4884 | CGC |
| n566 | BPG8 | Bhagwati Gupta |
| sy634 | PS3628 | Paul Sternberg |
| sy534 | PS2658 | Paul Sternberg |
| sy533 | PS2657 | Paul Sternberg |
| sy251 | PS1174 | Paul Sternberg |
| rh299 | VH12 | Harald Hutter |
| rh399 | VH24 | Harald Hutter |
| ps1 | HV74 | Wendy Hannah-Rose |
| ty6 | AN63 | Paul Sternberg |

**Table 3-** List of *lin-11* mutant alleles that are used in this study. *Caenorhabditis Genetics Center* (CGC).

| Locus | Oligo | Orientation | Sequence (5' to 3') |
|---|---|---|---|
| *rrf-3* | GL569 | Up | CTCCGAGTTCGCATCAAGTTTCAC |
| | GL570 | Down | GTCGTCTCTCTCCATTCCAGCTAATC |
| *eri-1* | GL571 | Up | GATTTCGAGTGTACGTGCGTCGAG |
| | GL572 | Up | CAGGCACTTTATCGAATATTC |
| | GL573 | Down | GAACTCTCGTCGTGTCACAGAG |
| *lin-11* | GL641 | Down | ACTGTATGTGGGATTTGTTGGGAGG |
| | GL642 | Up | GTCAATAACTCCGCCCATCAACC |
| | GL643 | Down | CATGTGTTCAGGCTCACTTGTCTG |
| | GL650 | Up | TACTGCGAATCGTCACCCAC |
| | GL651 | Up | GGGATGTGTCCTGTTGTCACTCT |
| | GL652 | Up | CTCGTTGCGGAATGGACATACA |
| | GL653 | UP | TACAGAGGACCATTCGGAACT |
| | GL654 | UP | CAAGCTAGGTGCTGCCAAAG |
| | GL655 | Down | GTGAGAGATAGTGCATTTCGAGGA |
| | GL791 | Down | CTTGCAGCCCGGCTCTTTAT |
| *egl-17* | GL707 | Up | CCCCCGCATGCCCTCATCTCTTATATCGTCTG |
| | GL708 | Down | CCCCCTCTAGACGGTGTTCGTTGGAAGAAATC |
| *zmp-1* | GL705 | Up | CCCCCGCATGCGAAGGACGGCTCGTTGAACAG |
| | GL706 | Down | CCCCCTCTAGACTAGAAAATGGCCAATATGC |

**Table 4-** Cell-autonomous expression of vulval markers in wildtype and *lin-11(ps1)* animals

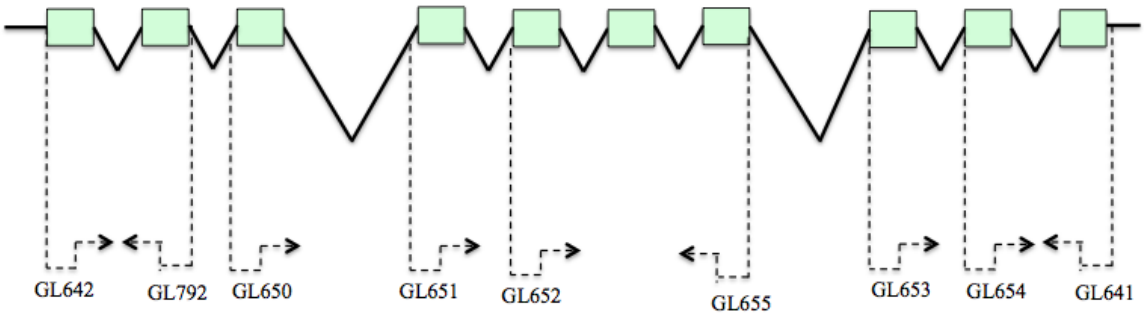


**Figure 13-** The position of *lin-11* primers is illustrated in this figure. Green boxes represents the exons and direction of arrow represents forward or reverse primers.

# Chapter 3- *lin-11* function in neuronal and epidermal cells

## 3.1 Structure-function analysis of *lin-11*

To better understand the function of *lin-11,* I initially sequenced several *lin-11* alleles. This information was expected to provide valuable information about the function of conserved domains in neuronal and vulval development. A total of eleven alleles were obtained from various sources (see Chapter 2 ; Table3). The results are shown in Table 5.

Five alleles have splicing deformities: *sy533, sy251*, *ty6*, *n566*, and *rh309*. In *sy533*, a point mutation converting a guanine nucleotide into an adenine nucleotide inactivates the 5' donor site of intron 1 at the junction of exon 1 and intron 1. In *sy251*, a point mutation converting a guanine nucleotide into an adenine nucleotide inactivates the 5' donor site of intron 3 at the junction of exon 3 and intron 4. Consequently, intron 3 is not spliced out during posttranscriptional modification and the conserved cysteine-rich LIM2 domain no longer functions properly. LIM domains are highly conserved between invertebrate and mammal systems and they also function in metal binding, protein-protein interaction and protein-nucleic acid interaction (Li et al., 1991). In the *rh309* allele a point mutation, within the 54-amino-acid region between LIM2 and HD, causes a guanine to adenine transition at the junction of exon 5 and intron 5; this occurs at the 5' donor site. Similarly, the point mutation in the *ty6* allele affects splicing at the 3' acceptor site of the junction between intron 1 and exon 2; thus, this mutation affects the conserved LIM1 domain. The *n566* allele was earlier sequenced by Dr. Gupta and was found to have a

deletion of 288 nucleotides affecting the junction of intron 4 and exon 5; in this case, the 3'acceptor site is deleted and the first nucleotide of exon 5 is absent, which affects the LIM2 domain. My data suggests that mutations affecting the acceptor or donor sites of the introns and exon junction in *lin-11* affect the overall structural integrity of the *lin-11* protein and abolish its correct function, causing vulva deformities.

The *sy534* allele has two missense mutations, one in exon 1 and one in exon 2, which affect the LIM1 and LIM2 domains, respectively. In exon 1, a valine is converted to an alanine – resulting in a nonpolar-to-nonpolar amino acid change – in position 36. In exon 2, the conserved cysteine residue of the LIM2 domain in position 125 is converted to tyrosine, a polar amino acid. The *sy634* allele has a missense mutation in exon 3, where the conserved cysteine residue of the LIM1 domain is converted to tyrosine in position 130. The fact that the mutations in both *sy534* and *sy634* affect the conserved cysteine residues of LIM domains suggests that those residues have important roles in the proper development of the vulva.

A point mutation in the *n382* allele changes a cytosine nucleotide to a thymine nucleotide and an arginine to a stop codon in position 165; which affects the LIM2 domain. This specific mutation produces a small transcript, completely abolishing the proper function of the *lin-11* protein. Similarly, the point mutation in the *rh299* allele converts a cytosine to a thymine and an arginine to a stop codon, in this case at position 257 inside the HD domain. However, as shown in Table 5, *rh299* is a weak *lin-11* allele, meaning that most of the animals with this mutation are able to lay eggs and have mostly

normal vulval morphology, which will be discussed in more detail. This finding suggests that *lin-11* is completely defective in *n382* and requires the HD and Pro domains for proper function; *rh299* affects the HD domain and affects only toroid finger protrusion in the vulva. The strong *n1281* mutant allele was found to have a 1.6 kb Tc1 transposon insertion in exon 7, which disrupts the structure and function of the homeodomain.

### 3.2 Vulva morphology and cell differentiation analysis

Next, I categorized the twelve sequenced *lin-11* alleles according to the severity of their vulval phenotypes. Three parameters are used to categorize them as weak, intermediate or strong alleles, as shown in Table 6. These parameters consist of proper vulva invagination, toroid finger protrusions and utse formation (Figure 14a). Nine alleles are categorized as intermediate in severity, meaning they have proper invagination but abnormal utse and toroid finger protrusion (Figure 14b). These eight alleles are also 100% egl, but are varied in terms of protruding vulva values (Table 6). *rh299* is the only allele that is categorized as weak, because the utse and vulva are not affected, though it contains one abnormality: variable toroid finger protrusions (Figure 14d, e, f). Thus, I decided to evaluate the severity of the toroid finger protrusions in *rh299*, as shown in Table 6. I have evaluated 30 *rh299* animals under Nomarski microscope, and all had toroid finger protrusion deformities, but vulva invagination and utse is not affected at all. Three alleles are categorized as strong *lin-11* alleles: *n389*, *n1281*, and *ty6*. These alleles are defective in all three categories (Figure 14b). Interestingly, some phenotypic characteristics, such as

protruding vulva, do not directly correlate with the severity of a given allele (Table 6). For example, the intermediate *n672* allele causes a protruding vulva in 75% of animals in 30 animals that I have evaluated, a much higher Pvl value than strong alleles. This finding suggests that the severity of an allele does directly correlate with the severity of the corresponding Egl phenotype.

To study the properties of developing vulval cells in *lin-11* mutant animals in more detail, I examined cell-type specific markers that are expressed in overlapping subsets of vulval cells. These include *egl-17* (fibroblast growth factor receptor homolog) and *zmp-1* (zinc metalloprotease) (Burdine et al., 1998; Inoue et al., 2002; Wang and Sternberg, 2000). I have generated two stable transgenic lines, DY425 and DY426, via a microinjection process in wildtype animals that show both *egl-17::CFP* and *zmp-1*::*YFP* expressions in their vulval cells. As illustrated in Table 7, 30 animals were observed under fluorescent microscope and only 40% of the wildtype animals showed *egl-17*::CFP expression in the late L4 stage in vulC and vulD progeny of the 2° lineages (Figure 15 a, b, e, f). Similarly, 43% of the animals had *zmp-1*::*YFP* expression in late L4 stage in vulE, and later in vulA (Figure 15 a, b, g, h). However, in *lin-11*(ps1) I find that the expression of *egl-17::CFP* was not present in vulC and vulD, nor was the expression of *zmp-1::YFP* presentin vulA, vulD and vulE, suggesting that these specific cells in the *ps1* allele did not acquire the correct identity (Table 7). In addition, similar findings have also been reported for *lin-11* null allele, n389; during the Pn.pxxx stage, the 2° lineage *egl-17* and *zmp-1* expressions was not detectable in vulval cells (Gupta et al., 2003).

### 3.3 Characterization of neuronal defect in *lin-11* animals

It has been shown that *lin-11* is expressed in and controls the differentiation of the pioneer neuron AVG (Hutter, 2003; T R Sarafi-Reinach et al., 2001). We were interested in expressing *odr-2::CFP* molecular marker, which encodes a Ly-6 superfamily protein; that, in turn, is expressed in sensory neurons, motor neurons, and interneurons (Cheu et al., 2001), in *n389* and *ps1* animals; this will allow me to further study the amphid sensory neurons in these mutant backgrounds. Specifically, I wantedto rescue the phenotypes of animals using three different plasmids, including: the control plasmid, pGF50, which contains the full length genomic sequence of *lin-11*; the second plasmid, pGLC70, which contains intron 7 of *lin-11* and drives the molecular expression of exons 8, 9, and 10 of *lin-11*; and the third plasmid, cDNA pGLC87, which contains intron 7 of *lin-11* and drives the expression of full length *lin-11* cDNA with *odr-2*::CFP as a neuronal molecular marker. *odr-2* expression is seen in 9 ± 2 neurons: AIZ, AIB, AVG, RIF, PVP, RIV, SIAV, IL2, ASG; it is faintly seen in SMD and RME (Chou et al., 2001). My results illustrate that *odr-2*::CFP expression is seen consistently in 10 neurons; however, expression is sometimes observed in 11 or 12 neurons in wildtype animals as well (Figure 16). In the *lin-11* null allele (*n389*) and in an intermediate allele, *ps1,* only 8 neurons consistently fluoresce brightly (Figure 17 c, d, g, h). This suggests that there are two neurons missing and that the only neurons for which *lin-11* function is required are AVG and AIZ. Thus, in all 23 animals analyzed for both *n389* and *ps1*, I did not observed any

CFP fluorescence in the AVG or AIZ neurons.

### 3.4 Characterization of electrotaxis defect of *lin-11* animals

The amphid neuronal expression of *lin-11* led us to examine the electrotaxis phenotype of *lin-11* mutants. Electrotactic behavior is mediated by certain amphid sensory neurons, ASH and ASJ, that are sensitive to the direction and strength of an electrical signal (Gabel et al., 2007). To study the mutants' electrotaxis behaviour, we used a microfluidic channel setup previously developed in our lab in collaboration with Dr. Selvaganapathy from Mechanical Engineering, McMaster University (Rezai et al., 2010 Lab Chip). This setup consists of a simple microchannel (300 mm wide, 80 mm deep, and 5 cm long) with electrodes at both end and a microscope equipped with a camera to record the behaviour of the animals. The average speed and turning response (as defined by Salam et al., manuscript submitted) of animals was analyzed. The turning response of wildtype L3 stage animals was 10.2 s while 23 *n389* animals took an average of 49.2 s to turn around (Figure 18). Furthermore, the calculation of the average *n389* turning time excludes four animals that did not respond to the electrical field at all. The average speed for N2 at the late L3 stage was 140 μm/s, which supports previously reported results (Rezai et al., 2010). On the other hand, *n389* mutants averaged 76 μm/s, which is an almost 50% reduction in speed when compared to the wildtype (Figure 19). I tested another mutant, *him-8* (with High Incidence of Males), to show that only mutations affecting muscles and neurons can be detected by the electrotaxis assay. While *him-8* is essential for proper meiotic segregation of the X chromosomes, it plays no direct role in

the normal development of muscles and neurons (Wong et al., 2005). The average speed of 15 *him-8* mutant animals was 131.4 um/s and the turning time averaged 9.6 s; both results were similar to wildtype animals (Figure 18 &19).

These results demonstrate that the electrotaxis defect in *lin-11* mutants is due to abnormalities in the amphid sensory neurons. Interestingly, some *lin-11* mutant animals seem to be able to detect field polarity changes, as they freeze for a few milliseconds in response; however, most neither responds nor moves in the correct direction, suggesting that the neurons responsible for detecting the changes are only partially functional. Furthermore, those animals that do respond and move when the field is activated usually move in the wrong direction, towards the anode, or gradually become completely paralyzed; when the polarity is switched, most cannot turn immediately or fail to turn at all and continue swimming in the wrong direction.

### 3.5 Dissection of intronic enhancers of *lin-11*

Previous work in our lab has shown that two of the largest introns of *lin-11*, introns 3 and 7, have enhancer regions used for neuronal regulation. Using the bioinformatics program Mussagl v.1.0.0 (http://woldlab.caltech.edu/~king/mussagl_manual/), I performed a 4-way comparison of the *lin-11* sequences found in four closely related *Caenorhabditis* species: *C. elegans, C. briggsae, C. remanei* and *C. brenneri* (Figure 20 & 21). A similar approach was previously taken to examine the 5' enhancer of *lin-11* and was shown to successfully

identify important functional elements (Marri and Gupta, 2009). Our analysis indicates that there are four regions of highly conserved blocks of nucleotide sequences when the window and threshold are set to a minimum of 70% conservation (or, a threshold of 21 and window of 30: 21/30= 70%). Three highly conserved regions are located at the 3'end of intron 3 while one is located at the 5' end (Figure 20a), However, among all four species, when the threshold is set to 90% conservation, only one block at the 3' end is conserved (Figure 20b). Similarly, the sequence alignment for intron 7 of *lin-11* between these four species is also shown in Figure 21. When the window and threshold were set to a minimum of 70% conservation (threshold of 21 and window of 30), the software indicated three conserved blocks of nucleotides at the 5' end of the intron (Figure 21b). Again, however, as the threshold is increased to 90% conservation the number of conserved blocks decreases (Figure 21a). We also compared the intron 3 and intron 7 sequences of just *C. elegans* and *C. briggsae*. This analysis showed eight conserved blocks of nucleotides in intron 7, at the 5' end, using 70% conservation (Figure 21d). When conservation is increased to 90%, four conserved regions remains (Figure 21c). One of these regions lies at the 3' end, so we hypothesized that it may be the promoter sequence for exon 8; the three other regions are found in the first half of the intron. Thus, we used the 5' end conserved site and the 3' end conserved site and split intron 7 into two parts.

Intron 3, 1355 bp in length, is expressed in ten head neurons while intron 7, 1284 bp in length, is expressed in two head neurons (Figure 22). A summer student in our lab,

Alem Adatia, had earlier made a plasmid containing full intron 3 sequences, pGLC59, and obtained three transgenic lines which all had similar expression patterns consisting of ten ventral cord neurons at different focal planes, as observed under a Nomarski microscope (Figure 22e). Another undergraduate thesis student, Asad Siddiqui, made a plasmid containing the *C. briggsae lin-11* homologue of intron 3, pGLC61, and obtained two transgenic lines, DY293 and DY351, showing expression patterns similar to those with pGLC59, DY243 and DY244. This finding suggests that intron 3 of *lin-11* is conserved between these two *Caenorhabditis* species. Analyzing cell bodies and axonal projections in order to identify these neurons under the Nomarski was difficult due to the neurons being located in different focal planes; a confocal microscope was employed to overcome this problem (Figure 22f). This approach was helpful in revealing both neuronal cell bodies and axonal projections. I have counted the total number of neurons and, with some confidence, the identity of individual cells. In the future, I plan to use specific neuronal markers to carry out double labeling experiments with *lin-11::GFP* to precisely determine neuronal identities.

We focused on intron 7 for further analysis because of its regulatory specificity and simple expression pattern, it being expressed in only two head neurons. We split intron 7 into two segments to determine the location of the possible enhancer and promoter elements. For each plasmid we generated two or more stable transgenic lines to avoid any microinjection bias that could result from the introduction of foreign plasmids (Table 8). The first plasmid, pGLC58, which consists of a pPD96.67 backbone and the

entire intron 7 sequence, including 30 bp of exon 7 and 74 bp of exon 8, showed expression in the AVG neuron as well as in a second neuron (Figure 23). Furthermore, the Mussagl software predicted blocks of conserved nucleotide sequences at the 5' end of intron 7, we generated pGLC65, which contains 30 bp of exon 7 and 568 bp of the 5' end of intron 7; this sequence showed an expression pattern similar to that of the full intron 7 sequence of pGLC58 (Figure 23; Table 8). The second plasmid contains the second part of intron 7, consisting of 986 bp, with a 98 bp overlap with pGLC65; this sequence showed no expression in the AVG neuron in both stable transgenic lines. Both pGLC65 and 66 were made from a pPD107.94 backbone, which contains a GFP molecular marker with a minimal promoter but no enhancer. We also inserted the 986 bp of intron 7 into the pPD95.67 vector series to create pGLC75, which contains GFP but no promoter or enhancer; we did this to discover if this segment has both promoter and enhancer regions. In fact, this turned out to be the case.

Next, I performed confocal imaging of pGLC50, which carries full intron 7 sequences, to create the visualizations of neuronal cell body positions and axonal projections needed to identify these neurons more accurately. In the case of intron 7, it was difficult to clearly determine the number and placement of the cells using a Nomarski microscope. Confocal images showed one cell body fluorescing in the junction between the posterior pharyngeal bulb and the intestine, with the axon extending posteriorly. This expression pattern is similar to that of the AVG neuron identified by Asad Siddiqui under a Nomarski microscope (Figure 22a, b, c; Table 8).

### 3.6 Rescue of *lin-11* phenotype by transgene expression

Next, we hoped to rescue the neuronal phenotype of *lin-11* using a full *lin-11* length cDNA plasmid, pGF50, as the control. pGF50 contains a 19 kb subclone of cosmid ZK273, which has been shown by Richard Durbin to rescue the *lin-11* phenotype (Durbin, PhD thesis University of Cambridge, 1987). My results are consistent with Durbin's findings in that pGF50 rescues the AVG neuron and the vulva phenotypes in *n389* animals (Figure 17e, f) (Durbin, PhD thesis University of Cambridge, 1987). Rescued *n389* animals were able to lay eggs and, significantly, were found to consistently express fluorescence in 10 neurons, as compared to the 7 that normally fluoresce in *n389*. This data confirms that *lin-11* expression is required for the development of the AVG and AIZ neurons.

Furthermore, we wanted to determine the activity of the small transcript of *lin-11,* which includes exons 8, 9 and 10 of the *lin-11* cDNA. We made a plasmid, pGLC70, in which intron 7, which contains enhancer activity, drives the molecular expression of exons 8, 9, and 10 of *lin-11*; we then attempted to rescue the AVG neuron in *lin-11* null mutants. My results illustrate that AVG was not rescued in *ps1*, as only 7-amphid neurons expressed fluorescence (Figure 17g, h). Therefore, the function of this small transcript, if it has one, is still unknown.

I also made a plasmid, pGLC87, in which intron 7 controls the expression of the entire *lin-11* cDNA sequence. I am interested to see whether this plasmid is capable of rescuing the AVG interneuron in the future.

### 3.7 RNAi screen for regulators of *lin-11*

We were interested in using RNA interference (RNAi) to identify transcription factor(s) and enhancer regions that might regulate the expression of *lin-11* in neurons. Although it has been shown that neurons in wildtype *C. elegans* are refractory to RNAi, it has been reported that many different RNAi-hypersensitive mutants do allow RNAi to be performed in the neurons (Simmer et al., 2002). Some of the genes conferring hypersensitivity when mutated include *lin-35, eri-1, rrf-3,* and *lin-15b* (Timmons et al., 2004; Simmer et al., 2002; Schmitz et al., 2007; Poole et al., 2011).

We especially intended to identify the enhancer region of intron 7 that regulates the expression of *lin-11* in the AVG neuron. Since neurons in wildtype *C. elegans* are refractory to RNAi, I created an *eri-1;rrf-3* double mutant from a cross of RNAi-hypersensitive *eri-1* and *rrf-3* mutants (Chapter 2 Figure 7). I speculated that this double mutant strain, named DY387, should be more sensitive to RNAi than the single mutants. I selected six genes known to have distinctive phenotypes in these mutant backgrounds to test the sensitivity of DY387; however, my findings, found in Table 9, do not show any significant difference in RNAi sensitivity between the single and double mutants. For example, *unc-86* encodes the POU transcription factor, which causes locomotion variability when the double-stranded RNA (dsRNA) is fed to these hypersensitive mutants (Baumeister et al., 1996). Our results illustrate that *rrf-3* does not show this uncoordinated phenotype: all animals on the RNAi plates had normal phenotypes with unaffected locomotion. This finding suggests that *rrf-3* is not an effective hypersensitive

mutant for this particular gene. On the other hand, 55% of *eri-1* animals show strongly uncoordinated locomotion, similar to the 65% penetrance in DY387; this suggests that the double mutant's hypersensitivity is similar to that of the single mutant. Similar findings were also seen in *dpy-13* RNAi knockdown experiments, in which 70% of DY387 animals, 62% of *eri-1* mutants and 24% of *rrf-3* mutants showed a strong dumpy (dpy) phenotype. However, the double mutants showed high sensitivity to RNAi against *unc-22*, *unc-119* and *unc-18*, compare to the single mutants as shown in Table 9. However, none of the mutants responded to *lin-1* RNAi, which has been reported to cause a multi-vulva phenotype (Schmitz et al., 2007).

Since the DY387 strain does not show robustly high RNAi sensitivity, we decided to use another well known RNAi-hypersensitive double mutant, *eri-1; lin15b* (Poole et al., 2011; Schmitz et al., 2007). I microinjected the plasmid carrying the full-length intron 7, pGLC58, into a *eri-1; lin15b* background to create the DY405 stable transgenic line, which expresses GFP in the AVG neuron. In addition, a similar transgenic line was obtained using the intron 3 plasmid, pGLC59, for future RNAi studies.

I generated a list of 120 transcription factors (TFs) that may bind to intron 7 of *lin-11* and regulate its expression in the AVG interneuron using MatInspector Genomatrix v. 8.0.0. The MatInspector program provided a large list of TF families specific to other organisms, as well as a list of 998 known TFs specific to *C. elegans*. I narrowed the list down to 120 TFs that fall under specific families (Haerty et al., 2008). My goal is to complete a preliminary round of RNAi testing using the 120 TFs that MatInspector

predicted, and later repeat this experiment on the TFs whose knockdown reduced fluorescence in AVG by 50% or more. So far, we have tested 39 TFs using the DY405 strain (Table 10). For example, while the L4440 control has 72% fluorescence in the AVG neuron, the *dmd-5* mutant has only 16% fluorescence in AVG, which suggests that knockdown of this TF reduces the expression of AVG by more than 70%. This finding suggests that DMD-5 may be one TF, among others, that regulates *lin-11* expression in AVG (Figure 24).

| Allele | Type | Position | Nucleotide | AA | Domain | AA Change | AA Position | Reference |
|---|---|---|---|---|---|---|---|---|
| rh299 | PM | Exon 6 | C→T | Stop | HD | Arg257Stop | 257 | This Study |
| rh309 | PM | Exon 5-Intron 5 Junction | G→A | N/A | LIM2--HD | Splicing Deformities | 5' Donor Site | This Study |
| sy251 | PM | Exon 3-Intron 3 Junction | G→A | N/A | LIM2 | Splicing Deformities | 5' Donor Site | This Study |
| sy533 | PM | Exon 1-Intron 1 Junction | G→A | N/A | N/A | Splicing Deformities | 5' Donor Site | This Study |
| sy534 | PM | Exon1<br>Exon2 | T→C<br>G→A | V→A<br>C→Y | N/A<br>LIM1 | Nonpolar→Nonpolar<br>Polar→Polar | 36<br>125 | This Study |
| sy634 | PM | Exon3 | G→A | C→Y | LIM2 | Polar Neutral→ Polar Aromatic | 130 | This Study |
| ty6 | PM | Intron 1-Exon 2 Junction | G→A | N/A | LIM1 | Splicing Deformities | 3' Acceptor Site | This Study |
| n382 | PM | Exon3 | C→T | Stop | LIM2 | Arg165Stop | 165 | This Study |
| n566 | Del | Intron 4-Exon 5 Junction | 288AA | N/A | LIM2 | N/A | 5' Donor Site | This Study |
| n672 | Del | | | **NC** | Pro | | | This Study |
| n1281 | Tc1 | Exon7 | N/A | N/A | HD | Tc1 transposon Insertion | N/A | This Study |
| ps1 | PM | Exon8 | G→A | V→M | Pro | Nonpolar→Nonpolar | 287 | Nelms and Hanna-Rose et al., 2006 |
| ok5023 | PM | Exon1 | C→T | T→T | LIM1 | Polar→ Polar | 36 | Flibotte et al., 2010 |
| zh41 | PM | Exon7 | C→T | L→F | HD | Nonpolar→Nonpolar | 274 | Zipperlen et al., 2005 |
| tm5323 | Del | Exon3 | 150bp | N/A | LIM2 | N/A | N/A | Shohie Mitani Lab |

**Table 5-** This table illustrates the characteristics of *lin-11* mutant alleles that were found in this study and other studies after sequencing the mutant allele. Not complete (NC) and not applicable (N/A).

| Allele | # Animals | Morphology | UTSE | % Egl | % Pvul |
|---|---|---|---|---|---|
| *rh299* | 30 | W | + | 0% | 10% |
| *rh309* | 30 | I | - | 100% | 23% |
| *sy533* | 30 | I | - | 100% | 67% |
| *sy534* | 30 | I | - | 100% | 46% |
| *sy634* | 30 | I | - | 100% | 54% |
| *sy251* | 30 | I | - | 100% | 35% |
| *n566* | 30 | I | - | 100% | 13% |
| *n382* | 30 | I | - | 100% | 67% |
| *n672* | 30 | I | - | 100% | 75% |
| *ps1* | 30 | I | - | 100% | 67% |
| *n1281* | 30 | S | - | 100% | 47% |
| *ty6* | 30 | S | - | 100% | 67% |
| *n389* | 30 | S | - | 100% | 53% |

**Table 6-** List of *lin-11* mutant alleles and their vulva morphological characteristics. (W) weak, (I) intermediate, (S) strong alleles and (Egl) egg-laying defect.

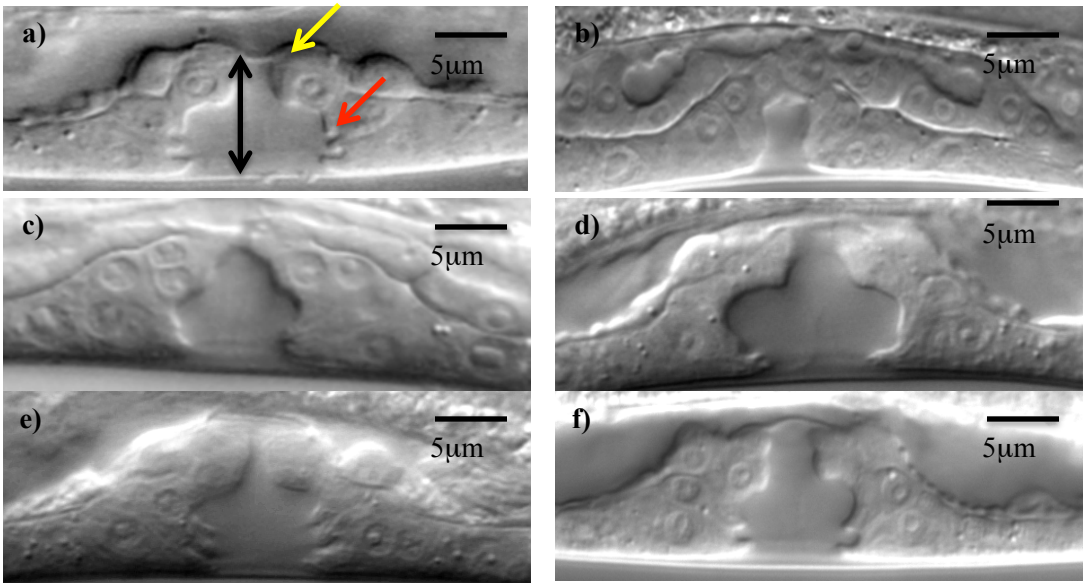


**Figure 14- Vulva morphologies.**

(a) Illustrating the vulva morphology of the wildtype animals. Black double headed arrow indicating vulva height, red arrow indicating toroid finger protrusions and yellow arrow indicating the utse. b) vulva morphology of *lin-11* null allele n389. c) Illustrating the vulva morphology of *lin-11* intermediate allele ps1. (d, e, f) illustrating the variation of vulva morphologies that are seen under Nomarki microscope in the weak *lin-11* allele rh299. *rh299* animals lay eggs and most have normal vulva phenotype as shown in (4c).

| | | *egl-17::CFP* | | *zmp-1::YFP* | |
|---|---|---|---|---|---|
| Strain | #Animals | vulC | vulD | vulA | vulE |
| DY425 (*N2*) | 30 | 40% | 40% | 43% | 43% |
| DY418 (*ps1*) | 30 | 0% | 0% | 0% | 0% |

**Table 7-** Cell-autonomous expression of vulval markers in wildtype (N2) and *lin-11(ps1)* animals.

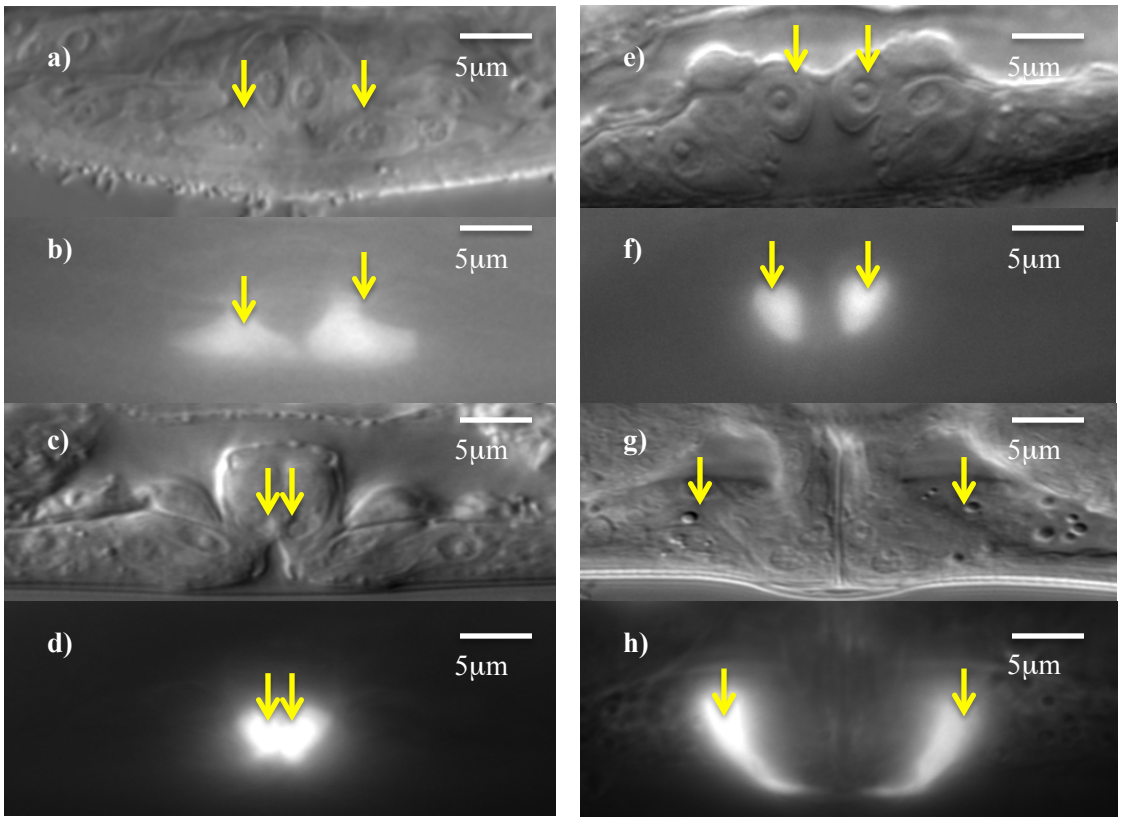


**Figure 15-** Expression pattern of the vulval markers in wildtype animals. (a,c,e,g) Nomarski images of the vulval cells. (b, f) Corresponding images showing *egl-17*::CFP fluorescence and (d, h) corresponds to *zmp-1*::YFP expressions. (a,b) wildtype *egl-17::GFP* expression in pairs of vulC cells shown by the arrows. (c,d) illustrates the YFP expressions in pair of vulE as shown by the arrows. (e, f) *egl-17*::CFP expression in pairs of vulD. And (g, h) corresponds to *zmp-1::YFP* expression of vulA in wildtype animals.

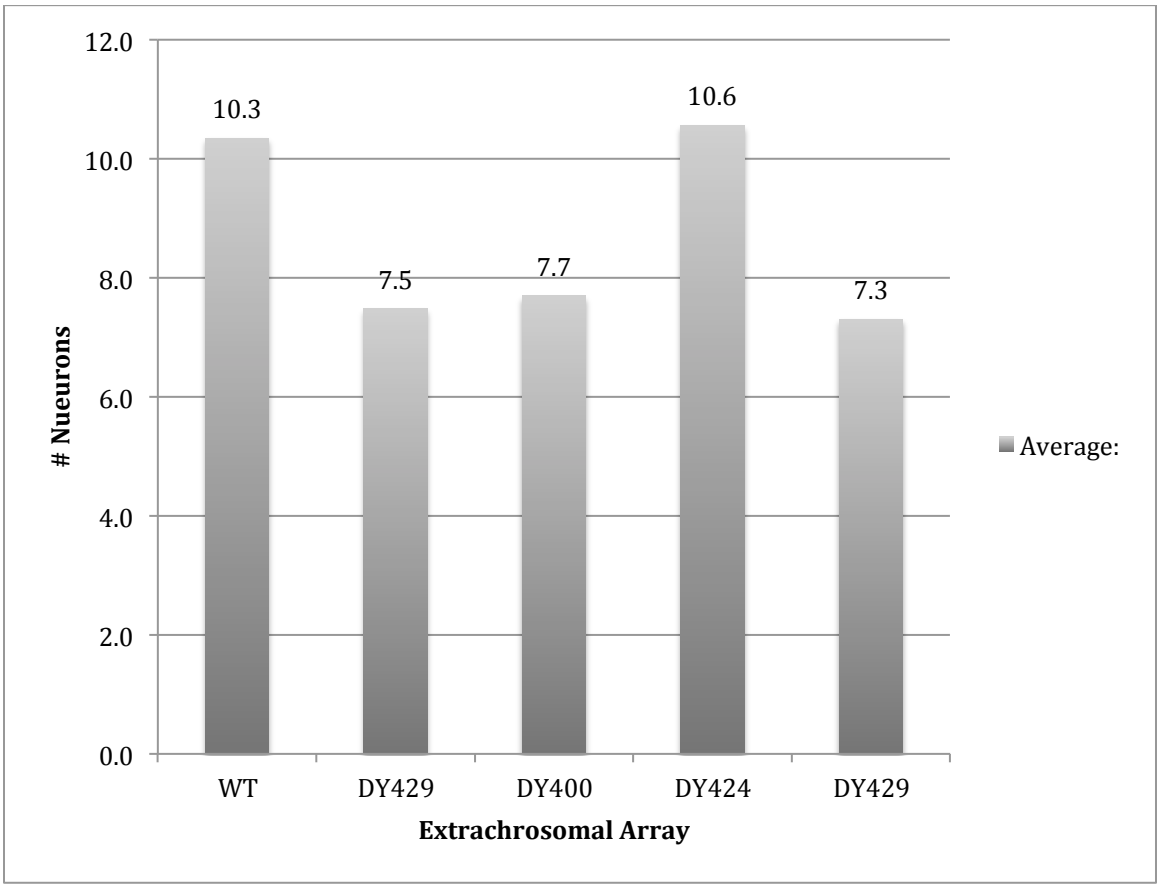


**Figure 16- *odr-2*::CFP neuronal marker expression**

Number of amphid sensory neurons that are observed in the WT animals, *lin-11* intermediate ps1 allele (DY429) and n389 null allele (DY400). Average number of neurons observed in n389 animals after microinjecting full-length *lin-11* plasmid pGF50 (DY424). DY429 illustrates the number of neurons that are observed when microinjecting pGLC70 plasmid into ps1 allele, which contains intron 7 driving the expression of exon 8, 9, and 10 of *lin-11*.

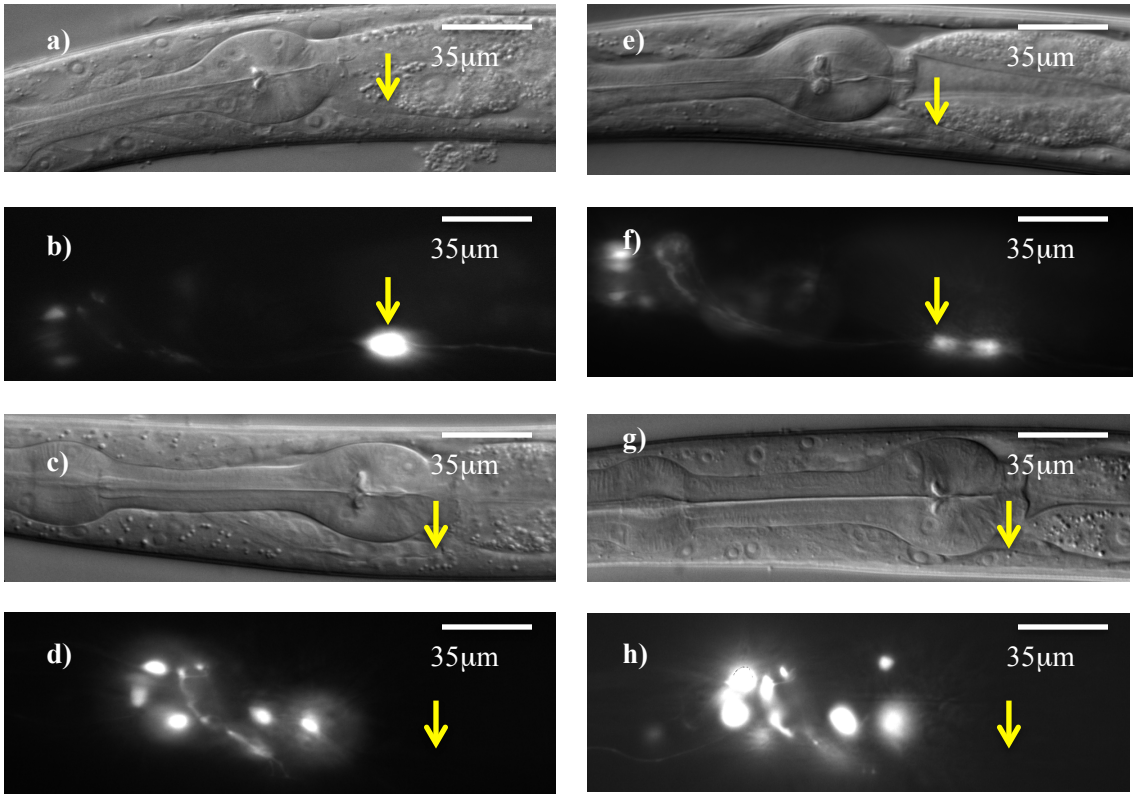


**Figure 17 – The expression of *odr-2::CFP* in the amphid sensory neurons.**

(a, c, e, g) correspond to the Nomarski images and (b, d, f, h) correspond to the CFP expressions. (a, b) illustrating the expression of *odr-2::CF*P in wildtype animals and the arrow indicating the position of the AVG neuron in wildtype animals. (c, d) illustrating *odr-2* expression in *lin-11* null allele n389, no CFP expression is seen in AVG neuron. (e, f) the expression of AVG is present after rescuing the n389 animals with pGF50 plasmid. (g, h) *odr-2* expression in the intermediate *lin-11* allele *ps1* and no AVG expression is seen in these animals which had similar expression to that of *n389.*

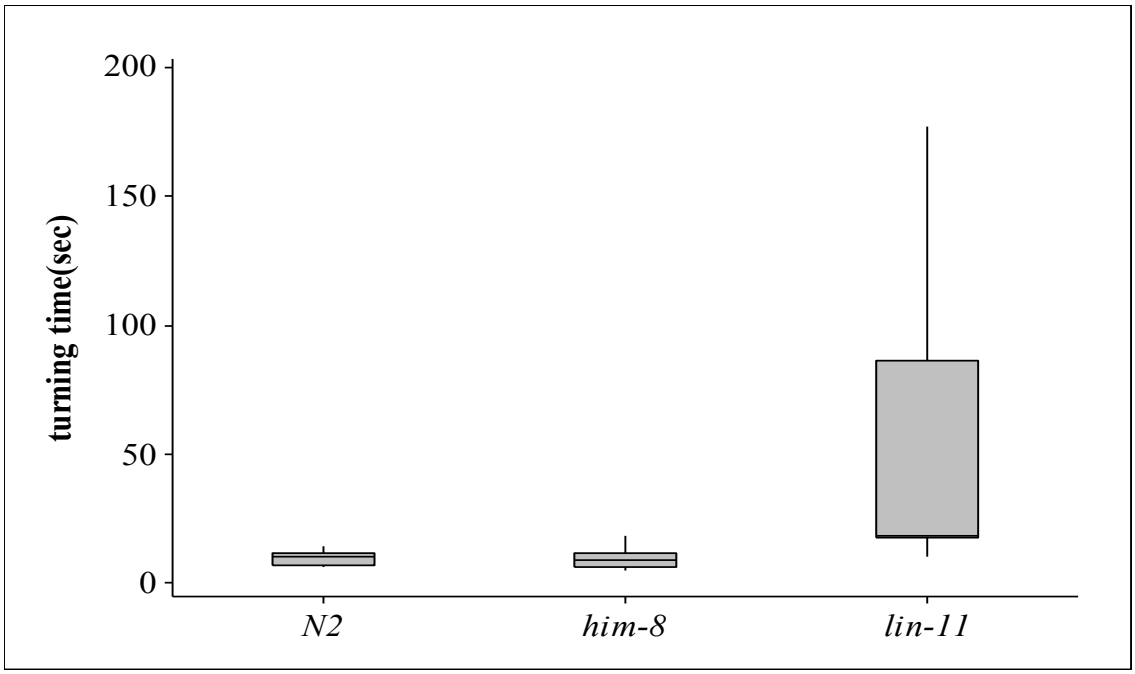


**Figure 18- Electrotactic analysis of the turning time**

We defined turning time the time it takes for these animals to turn their body 180$^{o}$ when electrical current changes in directions. Thus, the average turning time for *N2* was 10.2 sec and *him-8* was 9.6 sec. However, the average turning time for *lin-11* was 49 sec, which is four times slower than *N2* and *him-8*. In addition, *lin-11* box plot does not take seven animals turning time into consideration, because these animals did not respond to electrical current at all, and they were stationary at all times.

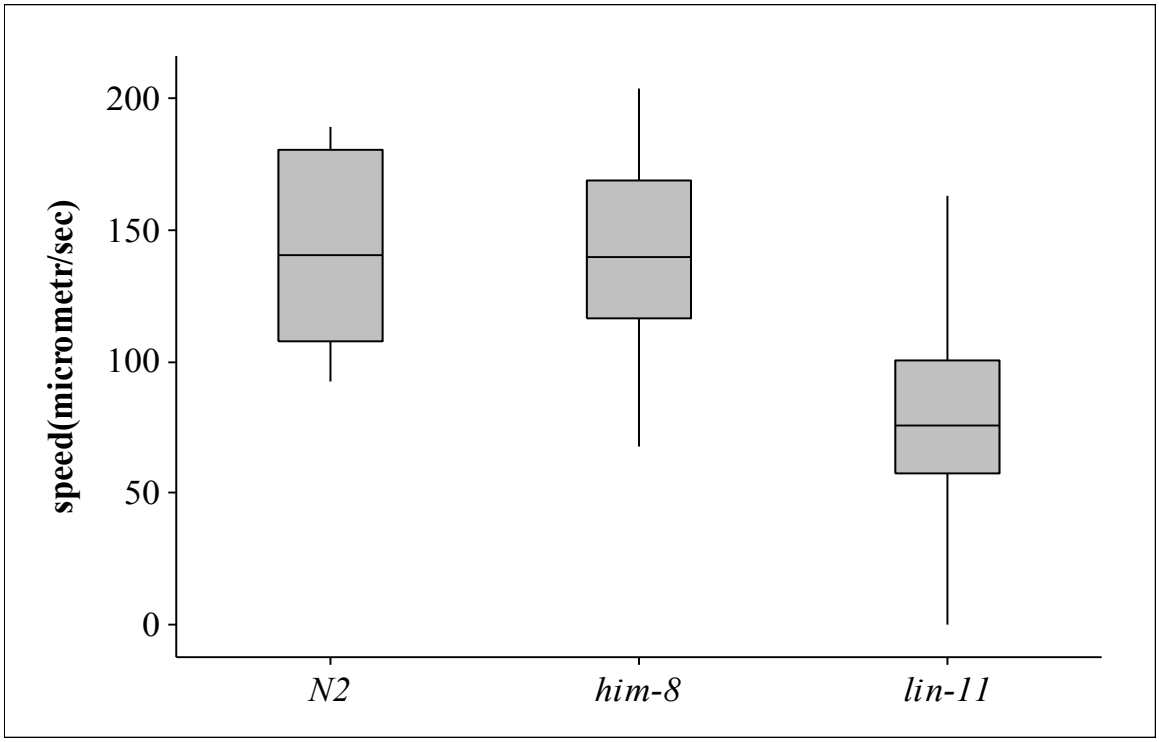


**Figure 19- Electrotactic analysis of the speed**

Box plot illustrating the speed of the *N2*, *him-8* and *lin-11* animals. The average speed of N2 is 140 µm/sec, which is almost similar to *him-8* at 131 µm/sec as expected. However, the average speed of *lin-11* animals is 76 µm/sec, which reduced to 50% compared to that of N2 and *him-8*. *lin-11* box plot does not take the speed of seven animals into consideration, because these animals did not respond to electrical current at all, and they were stationary at all times. This finding suggests that *lin-11* animals the amphid sensory neurons are defective and they do not communicating with the motor neurons or the muscles cells for proper locomotion response.

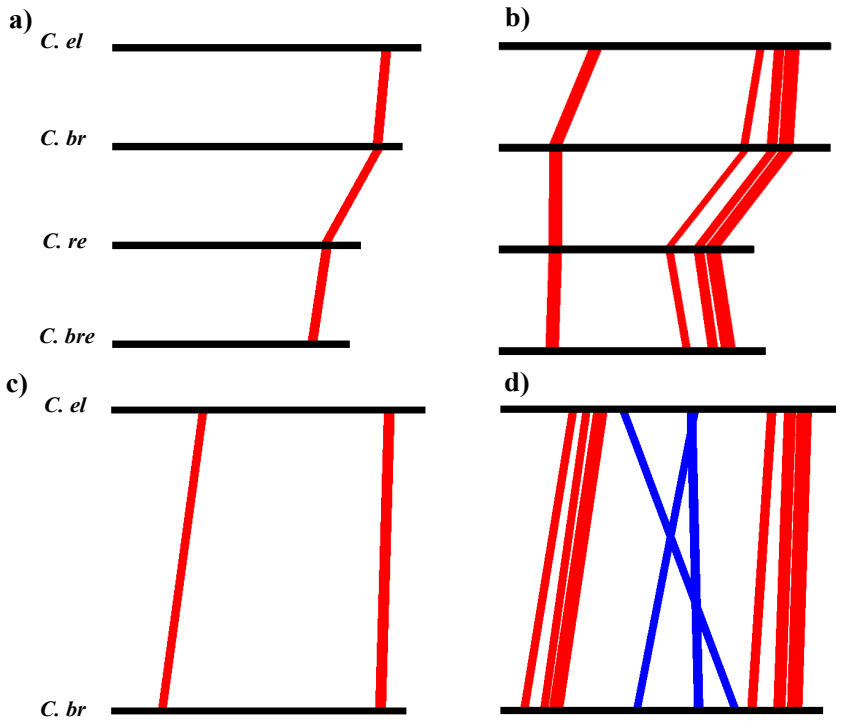


**Figure 20- Intron 3 sequence alignment between four closely related *Caenorhabditis* species.**

This figures illustrates the intron 3 sequence alignment using Mussagl v.1.0.0. bioinformatics program between four close species of Caenorhabditis, including *C.elegans* (*C.el*), *C. briggsae* (*C. br*), *C. remanei* (*C. re*) and *C. brenneri* (*C. bre*). Panel (a) shows 90% conservation between all four species, and only one small block of sequence is conserved amongst them, while in (b) 70% conservation and there are four regions are conserved. Alignment just between *C. el* and *C. br* with 90% conservation (c) shows two conserved regions, while eight conserved regions when the program set to 70% conservation between these sequences. Blue lines represent reverse complement conservation relative to the sequence attached to the top of the blue line.

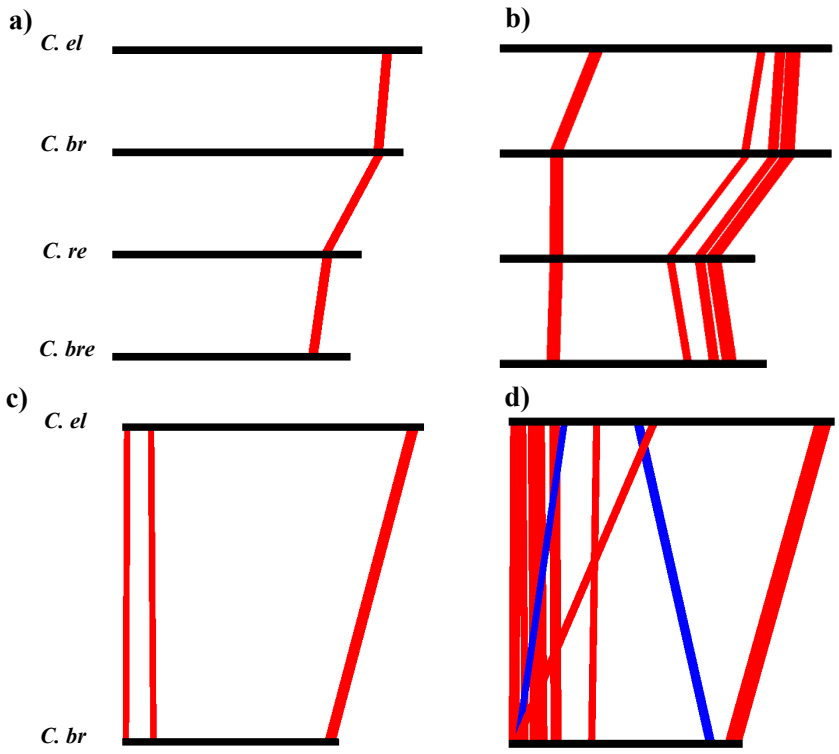


**Figure 21- Intron 7 sequence alignment between four closely related *Caenorhabditis* species.**

This figures illustrates the intron 7 sequence alignment using Mussagl v.1.0.0. bioinformatics program between four species of Caenorhabditis, including *C.elegans* (*C.el*), *C. briggsae* (*C. br*), *C. remanei* (*C. re*) and *C. brenneri* (*C. bre*). Panel (a) shows 90% conservation between all four species, and only one small block of sequence is conserved amongst them, while in panel (b) 70% conservation and four regions are conserved. Alignment just between *C. el* and *C. br* with 90% conservation shown in (c) where there are three conserved regions, while eight conserved regions when the program set to 70% conservation between these sequences. Blue lines represent reverse complement conservation relative to the sequence attached to the top of the blue line.

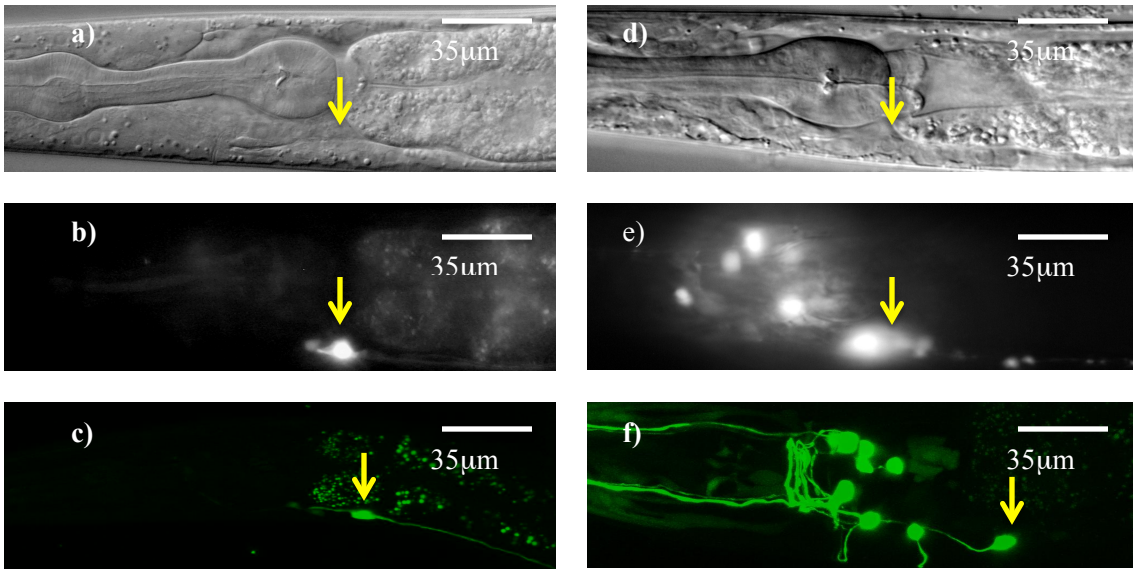


**Figure 22-** The neuronal expression pattern of intron 3 and intron 7 of *lin-11* in bhEx95 and bhEx98 transgenic strain respectively under the DIC and confocal microscopy. All arrows are indicating the position of AVG neuron. (a, d) corresponds to Nomarski images, (b, f) corresponds to the GFP expression of AVG neuron and (c, f) corresponds to the confocal images. (a, b, c) the expression pattern of full-length intron 7 and (d, e, f) the expression pattern of full-length intron 3.

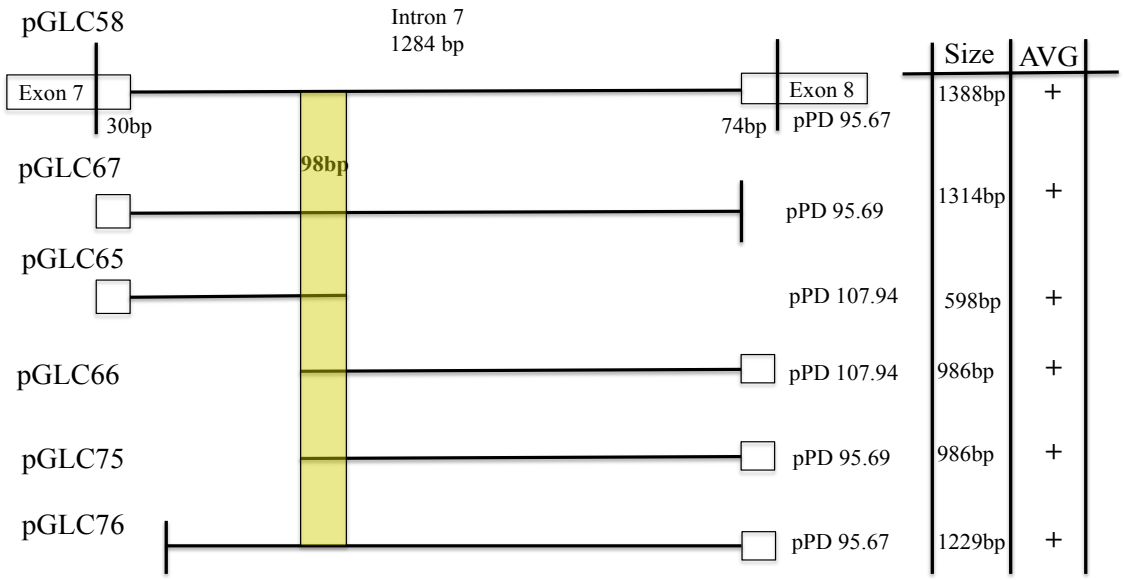


**Figure 23- Truncation of intron 7**

The expression of various plasmids was monitored in AVG neuron. This figure schematically illustrates the size and the name of each plasmid that were generated, and for each plasmid two or more transgenic stable lines were obtained via microinjection. Yellow highlighted region represents the conserved 98bp region, which the regulatory sequence may be located.

| Plasmid | Array # | Embryo | L1 | L2 | L4 | Adult | Second neuron | L4 Tail |
|---|---|---|---|---|---|---|---|---|
| pGLC58 | bhEx95 | 0/6 | – | – | 5/17 | – | 2/17 | 2/17 |
| | bhEx99 | 0/15 | 63/99* | – | 92/95[#] | – | 37/77[2] | 39/54[2] |
| pGLC60 | bhEx112 | 0/15 | 47/54* | 42/61[1] | 86/89[#] | – | – | – |
| | bhEx113 | 0/10 | 57/74[#] | 25/28[1] | 86/89[#] | – | 79/93[2] | 24/43[2] |
| | bhEx115 | 0/16 | – | – | – | – | 19/20 | 18/20 |
| pGLC65 | bhEx129 | 0/20 | 13/45[3] | – | 24/57[3] | – | 1/19 | 0/19 |
| | bhEx130 | 0/5 | 5/18[3] | – | 25/45[3] | – | 5/23 | 0/23 |
| pGLC66 | bhEx128 | 0/10 | 4/15 | – | 32/56 | – | – | 4/10 |
| pGLC75 | bhEx125 | 6/21 | 7/53 | – | 44/48 | 29/31 | 5/11 | 4/11 |
| | bhEx126 | 0/10 | 4/23 | – | 38/44 | 29/35 | 8/24 | 0/24 |
| pGLC76 | bhEx131 | 0/22 | 3/24 | – | 46/57 | – | 38/42 | 43/57 |
| | bhEx136 | 0/5 | 2/15 | – | 26/36 | – | 2/23 | 6/23 |

**Table 8-** This table illustrates number of transgenic stable lines that have been obtained for intron 7 of *lin-11* via microinjection for each plasmid. Array number is assigned to each transgenic stable line. Different larva stages have been observed and scored for the expression of AVG interneuron. In addition, analysis for other neurons in the head and tail is also have been scored.
*- Combined data of myself, Carly Ching and Asad Siddiqui
#- Combined data of Carly Ching and Asad Siddiqui
1- Asad Siddiqui's data
2- Carly Chings's data
3- Carly Chings and my data combined

| | **$N_2$** | | ***eri-1*** | | ***rrf-3*** | | **DY387** | | **Phenotype** |
|---|---|---|---|---|---|---|---|---|---|
| | Defect | Inter | Defect | Inter | Defect | Inter | Defect | Inter | |
| L4440 | 0% | 0% | 0% | 0% | 0% | 0% | 0% | 0% | None |
| *unc-22* | 15% (40) | 35% (40) | 0% | 24% (105) | 66% (155) | 23% (155) | 100% | 0% | Twitching |
| *unc-119* | 0% | 0% | 0% | 0% | 26% (135) | 41% (135) | 45% (145) | 24% (145) | Unc |
| *unc-86* | 0% | 0% | 55% (55) | 27% (55) | 0% (All) | 0% (All) | 65% (61) | 18% (61) | Unc Egl |
| *dpy-13* | 14% (55) | 15% (55) | 62% (130) | 23% (130) | 24% (106) | 1% (106) | 70% (71) | 16% (71) | Dpy |
| *unc-18* | 0% | 0% | 13% (115) | 35% (115) | 39% (64) | 9% (64) | 80% (40) | 20% (40) | Unc |
| *lin-1* | 0% | 0% | 0% | 0% | 0% | 0% | 0% | 0% | Muv |

**Table 9- Comparison of RNAi-hypersensitive strains**

This table illustrates quantification values of the unique phenotypically defect that was observed following RNAi knockdown of the in wildtype and single and double mutants of *eri-1*, *rrf-3* and *eri-1; rrf-3* (DY387). The value in the bracket represents number of animals scored in total for that specific gene, and phenotypes were divided into three categories including (inter) intermediate, strong (defective) and normal which is not shown. Defective animals showed very clear phenotype, however, intermediate phenotypes were hard to distinguish.

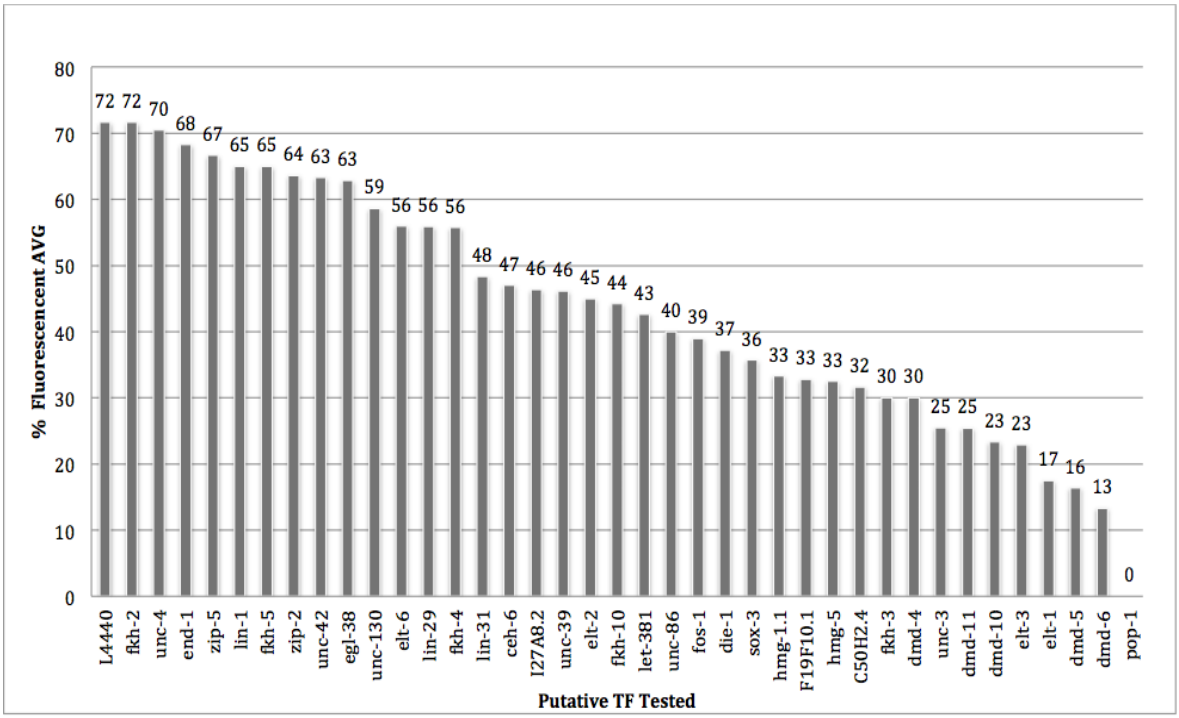


**Figure 24- RNAi analysis for putative transcription factors that regulate *lin-11* expressions in AVG neuron.**

List of 120 TF's was generated using MatInspector, however only 40 has been tested using hypersensitive RNAi mutant, DY405, to observe if it can knock down the molecular expression of GFP in AVG neuron. The value on top of the graph illustrates the percent of the animals that had AVG expression out however many that have been scored which is shown in Table 10.

| Gene | #Animals | AVG | % Fluorescence | Phenotype |
|---|---|---|---|---|
| L4440 | 60 | 43 | 72 | No Phenotype |
| *fkh-2* | 60 | 43 | 72 | Sick, sluggish |
| *unc-4* | 61 | 43 | 70 | Weak Unc |
| *end-1* | 60 | 41 | 68 | No Phenotype |
| *zip-5* | 21 | 14 | 67 | No Phenotype |
| *lin-1* | 60 | 39 | 65 | Weak Unc |
| *fkh-5* | 60 | 39 | 65 | No Phenotype |
| *zip-2* | 33 | 21 | 64 | No Phenotype |
| *unc-42* | 30 | 19 | 63 | Unc, sluggish |
| *egl-38* | 70 | 44 | 63 | Weak Egl, sluggish |
| *unc-130* | 58 | 34 | 59 | Locomotion Varient |
| *elt-6* | 50 | 28 | 56 | Embryonic arrest |
| *lin-29* | 93 | 52 | 56 | Pvul, sterile, Sluggish |
| *fkh-4* | 61 | 34 | 56 | No Phenotype |
| *lin-31* | 60 | 29 | 48 | Muv |
| *ceh-6* | 68 | 32 | 47 | Slow growth, larval lethal |
| *I27A8.2* | 41 | 19 | 46 | No phenotype |
| *unc-39* | 52 | 24 | 46 | Larval arrest |
| *elt-2* | 40 | 18 | 45 | Larval arrest |
| *fkh-10* | 61 | 27 | 44 | No Phenotype |
| *let-381* | 61 | 26 | 43 | Slow Growth, dumpy |
| *unc-86* | 60 | 24 | 40 | Locomotion varient, sluggish |
| *fos-1* | 77 | 30 | 39 | Pvul, sterile |
| *die-1* | 78 | 29 | 37 | Embryonic arrest, muv |
| *sox-3* | 28 | 10 | 36 | Sluggish, slow growth |
| *hmg-1.1* | 60 | 20 | 33 | Embryonic arrest, sluggish |
| *F19F10.1* | 61 | 20 | 33 | No Phenotype |
| *hmg-5* | 40 | 13 | 33 | Sterile, sluggish |
| *C50H2.4* | 60 | 19 | 32 | Sterile, sluggish |
| *fkh-3* | 60 | 18 | 30 | No Phenotype |
| *dmd-4* | 40 | 12 | 30 | No Phenotype |
| *unc-3* | 51 | 13 | 25 | Sluggish, slow growth |
| *dmd-11* | 59 | 15 | 25 | Slow growth |
| *dmd-10* | 60 | 14 | 23 | Slow growth |
| *elt-3* | 48 | 11 | 23 | Embryonic arrest |
| *elt-1* | 63 | 11 | 17 | Embryonic arrest |
| *dmd-5* | 61 | 10 | 16 | Slow growth, sterile |
| *dmd-6* | 30 | 4 | 13 | Slow growth, sterile |

| | | | | |
|---|---|---|---|---|
| *pop-1* | 0 | 0 | 0 | 100% Embryonic lethality |

**Table 10-** Table indicating the quantification of the phenotypes that were observed following RNAi knockdown of the potential putative transcription factors that was predicted by the bioinformatics program Matinspector. Using the hypersensitive mutant, DY405, to test if these TF's knockdown the expression of molecular marker, GFP, in AVG interneuron.

# Chapter 4- Conclusion and Future Direction

Regulation of gene interaction is critical for the proper development of animals to occur. In addition, multiple levels of regulation pathways cross talk is necessary to ensure that when one development process is affected the progression of others can continue. This multi-layered regulation is also required to terminate development if crucial process is missing or damaged. These communications are made possible via TF's, like *lin-11 that* regulates developmental processes. In this thesis, we have shown that two of the biggest intronic sequences of *lin-11* partake in regulatory activity. Specifically, we have demonstrated that intron 3 and intron 7 of *lin-11* produce the enhancer regulatory activity that is required for the proper development and function of amphid sensory head neurons. Using confocal and DIC microscopy, we have also identified some of these neurons using body positions and axon projections. These neurons have a variety of functions including: thermosensation, chemosensation, odorosensetion and mechanosensation. Since the intron 3 expression pattern was much more complex, we focused mainly in intron 7, which has a simple expression pattern that is only seen in two neurons. By truncating intron 7 we have illustrated that the 98 bp overlap between plasmid pGLC65 and pGLC66 may contain the regulatory sequence that is required for the proper function of AVG neurons. Because both pGLC65 and pGLC66 showed GFP expression in AVG neurons at different frequencies, two plausible hypothesis can be made: (1) both fragments of intron 7 have enhancer activity within their own sequences, and (2) the 98 bp overlap between these two plasmid contains the regulatory sequence required for the proper functioning of AVG

neurons. Thus, it was found that future work is required to generate one more plasmid that contains the 98 bp overlap. Furthermore, behavior analysis was carried out to demonstrate that *lin-11* animals are defective in proper locomotion.

Using electrotactic analysis, we have illustrated that *lin-11* null alleles are locomotory defective, a condition that can only arise when an the amphid sensory neurons are defective. We also tested another mutant, *him-8*, to rule out the possibility that all *C. elegans* mutations cause locomotion defective due to electrical stimuli that is applied in the microdevice. *him-8* speed was similar to that of the wildtype, which suggests that *lin-11* animals have defective amphid sensory neurons and that, as a result, their speed is much slower. However, some *lin-11* animals did detect the electrical stimuli but were unable to generate the correct response when the current's direction changed. In addition, turning time for *lin-11* was also much slower than that of the wildtype and *him-8* animals, further suggesting that locomotion variability was the result of defective sensory neurons. This finding suggests that sensory neurons are not communicating with motor neurons effectively and are not outputting the correct locomotive response to the electrical stimuli.

Sequencing *lin-11* alleles illustrated that the proper function of all conserved domains of *lin-11* are required for the proper function of the amphid sensory neuron and the development of vulva cells. Interestingly, rh299 does not follow this rule, because despite the point mutation that converts the amino acid arginine into a stop codon in position 257 and completely disrupts the HD and the overall structural integrity of the protein, it has a leaky phenotype; this means that these animals lay eggs and only 10% of

these animals show Pvul phenotype. Further observation of their vulva phenotype under the microscope detected only toroid finger protrusions; utse and vulva invagination was not disrupted. More work is required to determine how these animals are able to compensate for the defective *lin-11* protein, while other *lin-11* mutants, such as n1281 and rh309, which also have mutations in the HD, are unable to lay eggs and become Egl as a result of mutations.

We have identified a list of 120 putative TFs that may bind to *lin-11* enhancer sequences and regulate its expression in amphid sensory neurons, especially AVG, however, only 40 TFs have been tested and a couple TF families reduced the expression of GFP in AVG neurons by more than 50%, as shown in (Figure 14). We cannot confidently conclude that the TFs that did reduce the expression of GFP in AVG neurons are regulating the expression of AVG, because extra-chromosomal transgenic animals are not very reliable in terms of expression pattern consistency. The molecular expression pattern of the extra-chromosomal animals are not governed by the laws of Mandelian genetics, and thus not all F1 progenies will show fluorescence in the AVG neuron in our experiment; only 45% of the animals did. Thus, one can be misled 55% of the time if the lacking expression of GFP in AVG was the result of transcription factor knockdown or extra-chromosomal array inconsistency. Therefore, all 120 TFs need to be tested in the preliminary round, and a second round of RNAi needs to be performed to reconfirm the TFs that reduced the expression of GFP in AVG neurons by more than 50%; this should be done using integrated transgenic animals to avoid RNAi inconsistency and, more

importantly, to avoid dependency on certain phenotypes certain gene has; this way, confidently we can be sure that the GFP knock down was result of the RNAi not inconsistence in extra-chromosomal transgenic animals. Since GFP marker in all integrated animals follows the laws of Mandelian genetics, we can confidentially conclude that the knockdown in GFP expression in the AVG neurons in F1 progenies was the result of specific TFs.

In *lin-11* mutant animals, the AVG neuron is defective, as was shown by neuronal marker *odr-2*::CFP. In wildtype animals, ten head neurons expressed *odr-2*; however, in *lin-11* animals there were only 8 neurons present because the AVG and AIZ neurons were missing. To further support our findings, we rescued the *lin-11* phenotype using plasmid pGF50, which contains the full-length *lin-11* DNA sequence. As hypothesized, the rescued F1 progeny laid eggs, and the expression of ten neurons was also present, including that of the AVG and AIZ neurons (Figure 11e, f). Similarly, the tissue specific markers *egl-17* and *zmp-1* did not show expression in *lin-11* (ps1) vulval cells, which suggests that these tissues are completely defective. However, in wildtype animals the expression of *egl-17* is seen in vulC and vulD, while *zmp-1* expression is seen in vulA and vulE during late L4 stage. Thus, as shown here, the expression of *lin-11* is crucial to neurogenesis and vulval cell fate specifications.

### 4.1 Rescue analysis using domain specific plasmids

We have generated two plasmids, pGLC70 and pGLC78, which need to be microinjected into the *lin-11* null allele, n389, to determine if they can rescue the *lin-11* phenotype, including the AVG neuron and the vulva cells, using *odr-2::CFP* as a neuronal marker. pGLC70 contains intron 7, driving the molecular expression of exon 8, 9 and 10; it did not rescue the AVG neuron or the vulva phenotype in the intermediate allele, *ps1*. This plasmid should be microinjected into *n389* in order to rule out the possibility that the *lin-11* transcript is competing with pGLC70 in *ps1* animals and as result the phenotype was not rescued as a result. In *n389* animals no *lin-11* transcript is made, so it would show if this small transcript has a role in neuronal and vulval cell function. In addition, plasmid pGLC87 contains intron 7, driving the expression of full-length *lin-11* cDNA, which needs to be microinjected into *n389* as well to show if this plasmid is capable of rescuing *lin-11* phenotypes. Rescuing *lin-11* phenotypes using the plasmid pGLC87 is necessary to show that the function of all conserved *lin-11* domains is required for the proper function of amphid sensory neurons and vulval cells.

In addition, two other plasmids need to be generated to test the regulatory regions of intron 3. The first plasmid needs to be constructed in which intron 3 is driving the molecular expression of exon 4-10 of *lin-11* cDNA; the second plasmid should include intron 3 is driving the molecular expression of full-length *lin-11* cDNA. Both of these plasmids needs to be microinjected *lin-11* (n389) to illustrate if it has the capabilities to

rescue the *lin-11* phenotype, in order to confidently conclude the function of these transcripts of *lin-11* in the development of the neurons and vulval cells.

### 4.2 Chimeric homolog plasmids to rescue *lin-11* phenotype

*Lhx1* and *Lhx5* proteins (also called Lim1 and Lim5) are the two known vertebrate members of the *lin-11* group (Hobert and Westphal, 2000). Specifically, the function of *Lhx1* in Xenopus is required for proper neural induction in embryos, and, in the mouse, the head is severely compromised as result of this mutation (Shawlot and Behringer, 1995; Taira, M. et al., 1994). In mouse *Lhx5,* expression can be detected in the hypothalamus, which contains the main thermoregulatory processing centers of the brain (Sheng et al., 1997). *lin-11* function is also required for the proper functioning themosensory neurons in *C. elegans* as well. This raises one important question: can *Lhx1* and *Lhx5* rescue the *lin-11* phenotype in *C. elegans*? To answer this question, two plasmids that drive the expression of *Lhx1* and *Lhx5* under the native *lin-11* promoter could be tested for their ability to rescue the *lin-11* null phenotype.

# References

Bang, A G AG, and M D MD Goulding. (1996) "Regulation of Vertebrate Neural Cell Fate by Transcription Factors." Current Opinion in Neurobiology **6**(1), 25–32. Print.

Bargmann, C. I., Hartwieg, E., & Horvitz, H. R. (1993). Odorant-selective genes and neurons mediate olfaction in *C. elegans*. Cell, **74**(3), 515–527.

Bargmann, C. I., & Horvitz, H. R. (1991a). Chemosensory neurons with overlapping functions direct chemotaxis to multiple chemicals in *C. elegans*. Neuron, **7**(5), 729–742.

Bargmann, C., & Horvitz, H. (1991b). Control of larval development by chemosensory neurons in *Caenorhabditis elegans*. Science, **251**(4998), 1243–1246.

Bargmann CI, Mori I. Chemotaxis and Thermotaxis. In: Riddle DL, Blumenthal T, Meyer BJ, et al., editors. *C. elegans* II. 2nd edition. Cold Spring Harbor (NY): Cold Spring Harbor Laboratory Press; 1997.

Brenner, S. (1974). The genetics of *Caenorhabditis elegans*. Genetics, **77**(1), 71–94.

Broday L., Kolotuev I., Didier C., Bhoumik A., Gupta B.P., Sternberg P.W., Podbilewicz B., Ronai Z. (2004). The small ubiquitin-like modifier (SUMO) is required for gonadal and uterine-vulval morphogenesis in *Caenorhabditis elegans*. Genes Dev **18**(19), 2380–2391.

Cassata, G., Kagoshima, H., Andachi, Y., Kohara, Y., Dürrenberger, M. B., Hall, D. H., & Bürglin, T. R. (2000). The LIM homeobox gene *ceh-14* confers thermosensory function to the AFD neurons in *Caenorhabditis elegans*. Neuron, **25**(3), 587–597.

Chamberlin, H. M., Palmer, R. E., Newman, A. P., Sternberg, P. W., Baillie, D. L., & Thomas, J. H. (1997). The PAX gene egl-38 mediates developmental patterning in *Caenorhabditis elegans*. Development, **124**(20), 3919–3928.

Chang, C, A P Newman, and P W Sternberg. 1999. "Reciprocal EGF signaling back to the uterus from the induced *C. elegans* vulva coordinates morphogenesis of epithelia." Current biology: CB **9**(5): 237–246.

Chen, Ning, and Iva Greenwald. 2004. "The lateral signal for LIN-12/Notch in *C. elegans* vulval development comprises redundant secreted and transmembrane DSL proteins." Developmental Cell **6**(2): 183–192.

Chou, J. H., Bargmann, C. I., & Sengupta, P. (2001). The *Caenorhabditis elegans odr-2* gene encodes a novel Ly-6-related protein required for olfaction. Genetics, **157**(1), 211–224.

Cinar, H. N., Richards, K. L., Oommen, K. S., & Newman, A. P. (2003). The EGL-13 SOX domain transcription factor affects the uterine pi cell lineages in *Caenorhabditis elegans*. Genetics, **165**(3), 1623–1628.

Delattre, M., and M.A. Félix. 1999. "Connection of vulval and uterine epithelia in *Caenorhabditis elegans*." Biology of the Cell **91**(8): 573–583.

Durbin E. M. 1987. "Studeies on the development and organization of the nervous system of *C. eleganas*". Ph.D thesis. University of Cambridge, United Kingdom.

Eisenmann, D M, and S K Kim. 1994. "Signal transduction and cell fate specification during *Caenorhabditis elegans* vulval development.." Current Opinion in Genetics & Development **4**(4): 508–516.

Eisenmann, D. M., Maloof, J. N., Simske, J. S., Kenyon, C., & Kim, S. K. (1998). The beta-catenin homolog BAR-1 and LET-60 *Ras* coordinately regulate the *Hox* gene *lin-39* during *Caenorhabditis elegans* vulval development. Development **125**(18), 3667–3680.

Ferguson, E L, P W Sternberg, and H R Horvitz. (1987). "A genetic pathway for the specification of the vulval cell lineages of *Caenorhabditis elegans*." Nature **326**(6110): 259–267.

Gwendylyn Freyd Ann, (1991). "Molecular analysis of the *Caenorhabditis elegans* cell lineage gene *lin-11*", Ph.D thesis, Massachusetts Institute of Technology.

Freyd, G., Kim, S. K., & Horvitz, H. R. (1990). Novel cysteine-rich motif and homeodomain in the product of the *Caenorhabditis elegans* cell lineage gene *lin-11*. Nature, **344**(6269), 876–879.

FREYD, G., 1991 (Ph.d) Molecular analysis of the *Caenorhabditis elegans* cell lineage gene *lin-11*, pp. 159 in *Biology*. Massachusetts Institute of Technology, Boston.

Gabel, C. V., Gabel, H., Pavlichin, D., Kao, A., Clark, D. A., & Samuel, A. D. T. (2007). Neural Circuits Mediate Electrosensory Behavior in *Caenorhabditis elegans*. Journal of Neuroscience, **27**(28), 7586–7596.

Gupta, B. (2002). Tissue-Specific Regulation of the LIM Homeobox Gene *lin-11* during Development of the *Caenorhabditis elegans* Egg-Laying System. Developmental biology, **247**(1), 102–115.

Gupta, B. P., Wang, M., & Sternberg, P. W. (2003). The C. elegans LIM homeobox gene *lin-11* specifies multiple cell fates during vulval development. Development, **130**(12), 2589–2601.

Hanna-Rose, W W, and M M Han. 1999. "COG-2, a sox domain protein necessary for establishing a functional vulval-uterine connection in *Caenorhabditis elegans*." Development **126**(1): 169–179.

Hutter, Harald. (2003) "Extracellular Cues and Pioneers Act Together to Guide Axons in the Ventral Cord of *C. Elegans*." Development, **130** (22): 5307–5318.

Hutter, Harald et al. "Novel Genes Controlling Ventral Cord Asymmetry and Navigation of Pioneer Axons in *C. Elegans*." Developmental biology 284.1 (2005): 260–272.

Hobert O. Specification of the nervous system. 2005 Aug 8. In: WormBook: The Online Review of C. elegans Biology [Internet]. Pasadena (CA): WormBook; 2005-.

Hobert, O. O., D'Alberti, T. T., Liu, Y. Y., & Ruvkun, G. G. (1998). Control of neural development and function in a thermoregulatory network by the LIM homeobox *gene lin-11*. The Journal of neuroscience: the official journal of the Society for Neuroscience, **18**(6), 2084–2096.

Hobert, O., Tessmar, K., & Ruvkun, G. (1999). The *Caenorhabditis elegans* lim-6 LIM homeobox gene regulates neurite outgrowth and function of particular GABAergic neurons. Development (Cambridge, England), **126**(7), 1547–1562.

Hobert, O., & Westphal, H. (2000). Functions of LIM-homeobox genes. Trends in Genetics, **16**(2), 75–83.

Inoue, T., Wang, M., Ririe, T. O., Fernandes, J. S., & Sternberg, P. W. (2005). Transcriptional network underlying *Caenorhabditis elegans* vulval development. PNAS, **102**(14), 4972.

Jorgensen, E. M. (2005). GABA. WormBook. doi:10.1895/wormbook.1.14.1

Kirouac, Martha, and Paul W Sternberg. (2003). "cis-Regulatory control of three cell fate-specific genes in vulval organogenesis of *Caenorhabditis elegans* and *C. briggsae*." *Developmental biology* **257**(1): 85–103.

Kimble, J. J., & Hirsh, D. D. (1979). The postembryonic cell lineages of the hermaphrodite and male gonads in *Caenorhabditis elegans*. Developmental biology, **70**(2), 396–417.

Li, P. M., Reichert, J., Freyd, G., Horvitz, H. R., & Walsh, C. T. (1991). The LIM region of a presumptive Caenorhabditis elegans transcription factor is an iron-sulfur- and zinc-containing metallodomain. PNAS, **88**(20), 9210–9213.

Marri, S., & Gupta, B. P. (2009). Dissection of lin-11 enhancer regions in Caenorhabditis elegans and other nematodes. Developmental Biology, **325**(2), 402–411.

Mori, I. I., & Ohshima, Y. Y. (1995). Neural regulation of thermotaxis in *Caenorhabditis elegans*. Nature, **376**(6538), 344–348.

Newman, A P, J G White, and P W Sternberg. 1995. "The *Caenorhabditis elegans lin-12* gene mediates induction of ventral uterine specialization by the anchor cell.." Development (Cambridge, England) **121**(2): 263–271.

Newman, A. P., White, J. G., & Sternberg, P. W. (1996). Morphogenesis of the *C. elegans* hermaphrodite uterus. Development (Cambridge, England), **122**(11), 3617–3626.

Newman, A. P., Acton, G. Z., Hartwieg, E., Horvitz, H. R., & Sternberg, P. W. (1999). The *lin-11* LIM domain transcription factor is necessary for morphogenesis of *C. elegans* uterine cells. Development (Cambridge, England), **126**(23), 5319–5326.

Rezai, P., Siddiqui, A., Selvaganapathy, P. R., & Gupta, B. P. (2010). Electrotaxis of *Caenorhabditis elegans* in a microfluidic environment. Lab on a chip, **10**(2), 220–226.

Sengupta, P., Colbert, H. A., & Bargmann, C. I. (1994). The *C. elegans* gene *odr-7* encodes an olfactory-specific member of the nuclear receptor superfamily. Cell, **79**(6), 971–980.

Sagasti, A., Hobert, O., Troemel, E. R., Ruvkun, G., & Bargmann, C. I. (1999). Alternative olfactory neuron fates are specified by the LIM homeobox gene *lim-4*. Genes & Development, **13**(14), 1794–1806.

Sarafi-Reinach, T. R., Melkman, T., Hobert, O., & Sengupta, P. (2001). The *lin-11* LIM homeobox gene specifies olfactory and chemosensory neuron fates in *C. elegans*. Development (Cambridge, England), **128**(17), 3269–3281.

Scott, M. P., Tamkun, J. W., & Hartzell, G. W., III. (1989). The structure and function of the homeodoman. BBA Reviews on Cancer **9**, 25-48.

Sharma-Kishore R, White R J G, Southgate E, and Podbilewicz, B. 1999. "Formation of the vulva *in Caenorhabditis elegans*: a paradigm for organogenesis." *Development (Cambridge, England)* **126**(4): 691–699.

Shawlot, W. and Behringer, R.R. (1995) Requirement for Lim1 in head-organizer function. Nature 374, 425–430

Sheng, H.Z., Bertuzzi S., Chaing, C., Shawlot, W., Taira, M., Dawid, I., and Westphal, H. (1997) Expression of murine Lhx5 suggests a role in specifying the forebrain. Dev. Dyn. 208, 266–277

Sternberg, P W, and H R Horvitz. (1991). "Signal transduction during *C. elegans* vulval induction." *Trends in Genetics* **7**(11-12): 366–371.

Sherwood, David R, and Paul W Sternberg. (2003). "Anchor cell invasion into the vulval epithelium in *C. elegans*." Developmental Cell **5**(1): 21–31.

Sternberg, P. W. (2005). Vulva development. In WormBook, T.C.e.R Community, ed. (WormBook).

Stein, L. D., Bao, Z., Blasiar, D., Blumenthal, T., Brent, M. R., Chen, N., Chinwalla, A., et al. (2003). The genome sequence of *Caenorhabditis briggsae*: a platform for comparative genomics. PLoS biology, **1**(2), E45.

Sulston, J. E., & Horvitz, H. R. (1977). Post-embryonic cell lineages of the nematode, *Caenorhabditis elegans*. Developmental biology, **56**(1), 110–156.

Sulston, J. E. J., & White, J. G. J. (1980). Regulation and cell autonomy during postembryonic development of *Caenorhabditis elegans*. Developmental biology, **78**(2), 577–597.

Sundaram M.V. (2006). RTK/Ras/MAPK signaling. In WormBook, T.C.e.R Community, ed. (WormBook).

Taira, M., Otani H. H., Saint-Jeannet J. P., & Dawid I. B. (1994) Role of the LIM class

homeodomain protein X lim-1 in neural and muscle induction by the Spemann organizer in Xenopus. Nature 372, 677–679

Udin, S. B. S., & Fawcett, J. W. J. (1988). Formation of topographic maps. Neuroscience, 11, 289–327.

Vallee, B. L., Coleman, J. E., & Auld, D. S. (1991). Zinc fingers, zinc clusters, and zinc twists in DNA-binding protein domains. PNAS, **88**(3), 999–1003.

Velyvis A, Qin J. LIM Domain and Its Binding to Target Proteins. In: Madame Curie Bioscience Database [Internet]. Austin (TX): Landes Bioscience; 2000-. Available from: http://www.ncbi.nlm.nih.gov/books/NBK6372/

Voutev, R., Keating, R., Jane Albert Hubbard, E., & Vallier, L. G. (2009). Characterization of the *Caenorhabditis elegans* Islet LIM-homeodomain ortholog, *lim-7*. FEBS Letters, **583**(2), 456–464.

Wadsworth, W G, and E M Hedgecock. "Hierarchical Guidance Cues in the Developing Nervous System of *C. Elegans*." BioEssays: news and reviews in molecular, cellular and developmental biology **18.5** (1996): 355–362.

Wagmaister, J. A., Gleason, J. E., & Eisenmann, D. M. (2006). Transcriptional upregulation of the *C. elegans* Hox gene *lin-39* during vulval cell fate specification. Mechanisms of Development, **123**(2), 135–150.

Way, J. C. J., & Chalfie, M. M. (1988). *mec-3*, a homeobox-containing gene that specifies differentiation of the touch receptor neurons in *C. elegans*. Cell, **54**(1), 5–16.

Wong P. C. M., C., Bhalla, N., Carlton, P. M., Weiser, P., Meneely, P. M., & Dernburg, A. F. (2005). HIM-8 Binds to the X Chromosome Pairing Center and Mediates Chromosome-Specific Meiotic Synapsis. Cell, **123**(6), 1051–1063.

Xue, D. D., Finney, M. M., Ruvkun, G. G., & Chalfie, M. M. (1992). Regulation of the *mec-3* gene by the *C.elegans* homeoproteins UNC-86 and MEC-3. The EMBO journal, **11**(13), 4969–4979.